Protein aggregation as an antibiotic design strategy

Natalia G. Bednarska[1,2], Johan Van Eldere[1,*], Rodrigo Gallardo[2,3], Ashok Ganesan[2,3], Meine Ramakers[2,3], Isabel Vogel[4], Pieter Baatsen[5], An Staes[6,7], Marc Goethals[6,7], Per Hammarström[8], K. Peter R. Nilsson[8], Kris Gevaert[6,7], Joost Schymkowitz[2,3,*] & Frederic Rousseau[2,3,*]

[1] Laboratory of Clinical Bacteriology and Mycology, Department of Microbiology & Immunology, KULeuven, Belgium.
[2] Switch Laboratory, VIB, Leuven, Belgium.
[3] Switch Laboratory, Department of Cellular and Molecular Medicine, KULeuven, Belgium.
[4] Laboratory of Immunology, Department of Microbiology & Immunology, KULeuven, Belgium
[5] Department of Molecular and Developmental Genetics (VIB11 and KULeuven), Electron Microscopy Network (EMoNe), Gasthuisberg, Leuven, Belgium.
[6] Department of Medical Protein Research, VIB, Ghent, Belgium.
[7] Department of Biochemistry, Ghent University, Ghent, Belgium.
[8] Department of Chemistry, Linköping University, Linköping, Sweden.
* To whom correspondence should be addressed

Keywords: Antimicrobial peptide (AMP), protein aggregation, proteostasis, chaperone

Abstract

Taking advantage of the xenobiotic nature of bacterial infections, we tested whether the cytotoxicity of protein aggregation can be targeted to bacterial pathogens without affecting their mammalian hosts. In particular we examined if peptides encoding aggregation-prone sequence segments of bacterial proteins can display antimicrobial activity by initiating toxic protein aggregation in bacteria but not in mammalian cells. Unbiased *in vitro* screening of aggregating peptide sequences from bacterial genomes lead to the identification of several peptides that are strongly bactericidal against methicillin resistant *Staphylococcus aureus*. Upon parenteral administration *in vivo*, the peptides cured mice from bacterial sepsis without apparent toxic side effects as judged from histological and haematological evaluation. We found that the peptides enter and accumulate in the bacterial cytosol where they cause aggregation of bacterial polypeptides. Although the precise chain of events that leads to cell death remains to be elucidated, the ability to tap into aggregation-prone sequences of bacterial proteomes to elicit antimicrobial activity represents a rich and unexplored chemical space to be mined in search of novel therapeutic strategies to fight infectious diseases.

Introduction

The rapid global increase of antibiotic resistance signals the end of prevention-only measures to ward off the advent of the post-antibiotic era and underlines the urgent need for novel therapeutics (Gravitz, 2012). Naturally occurring and synthetic Antimicrobial Peptides (AMPs) are a very rapidly developing area of antibacterial research due to their fast and efficient killing ability (Nakatsuji & Gallo, 2012). Initially, antimicrobial peptides were considered as a uniform group of molecules that bind to and disrupt negatively charged bacterial membranes via clusters of positively charged and hydrophobic amino acids (Lee & Lee, 2014). In this classic view AMPs achieve membrane disruption through a number of mechanisms, including pore formation, transmembrane channel formation, insertion into lipid bilayer and disruption of the membrane lipid backbone. Such AMPs are predominantly broad-spectrum antibacterials and the major limitation of this broad-spectrum membrane-activity is that very often they do not display great specificity for bacterial membranes over their mammalian counterparts, which has been a limiting factor for their therapeutic applications. In recent years, it became apparent that the range of action mechanisms is more complex and often includes interaction with intracellular targets (Lee & Lee, 2014, Nguyen *et al.*). A number of antimicrobial peptides such as the proline-rich AMPs (Pr-AMPs) were shown to act on internal targets either as an additional effect to their membrane disruptive properties or exclusively as their major mechanism of action. These AMPs have a clear advantage in specific toxicity towards bacterial cells, rendering them much more suitable for therapeutic development; this is thought to be due to the uptake mechanisms of these peptides, which involve specific bacterial transporter proteins that are not present in Mammalia. Although their multi-target mode of action makes these AMPs difficult to study, it also may offer a striking advantage over conventional antibiotics, which mostly have a single target site that intrinsically renders them prone to rapid development of resistance.

A mechanism of action that has recently been proposed is the disruption of bacterial protein homeostasis or proteostasis (Balch *et al.*, 2008), potentially leading to toxic protein aggregation in the bacterial cell. For example, the primary target for the PrAMP oncocin and its derivatives is thought to be the

ribosome exit channel (Roy *et al.*, 2015, Seefeldt *et al.*, 2015), but these peptides are also known to bind to and inhibit the bacterial Hsp70 homolog DnaK (Knappe *et al.*, 2011), which will likely amplify the disruption of bacterial proteostasis of these peptides. Interestingly, many AMPs are known to form amyloid structure spontaneously (Zhao *et al.*, 2006, Mahalka & Kinnunen, 2009, Torrent *et al.*, 2011) and co-aggregation has been observed between AMPs and bacterial proteins (Code *et al.*, 2009). Moreover, it was recently shown that some known amyloidogenic peptides are indeed toxic to bacterial cells (Last & Miranker, 2013) and it was even proposed that the Alzheimer β-peptide may itself be an overlooked antimicrobial peptide (Soscia *et al.*, 2010). Introduction of positively charged amino acids in amyloidogenic peptides lead to the identification of novel AMPs, highlighting the overlap between both types of sequences (Torrent *et al.*, 2011). Since it is further known that heterologous seeding of protein aggregation is significantly less efficient than homologous seeding (Morales *et al.*, 2013), we speculated that aggregation-prone peptides whose sequences are derived from the aggregation prone regions of bacterial proteins could be used to induce toxic protein aggregation more efficiently in bacteria than in other organisms, potentially providing a new design paradigm for antimicrobial peptides. This is based on the idea that protein aggregation is mediated through the formation of intermolecular b-structures by short aggregation prone regions (APRs) of the polypeptide sequence (Esteras-Chopo *et al.*, 2005), which can be identified in polypeptide sequences by bioinformatic means (De Baets *et al.*, 2014). We have exploited the short-stretch hypothesis of protein aggregation to design so-called aggregator peptides with the aim of yielding more specific, intracellular bactericidal efficacy. The peptides were shown to induce specific aggregation of bacterial proteins. These peptides display a strong bactericidal effect against important human pathogens such as *Staphylococcus aureus* and *Enterococcus faecalis*, as well as their drug resistant derivatives (MRSA and VRE). We show that targeted aggregation can be a successful antimicrobial strategy due to its complex mechanism of action involving both intracellular activity and membrane perturbations.

Results

Design and rationale of aggregating antibacterial peptides

To test our hypothesis we identified aggregation prone regions (APRs) in the proteome of *Staphylococcus epidermidis* using the statistical thermodynamics algorithm TANGO (Fernandez-Escamilla *et al.*, 2004). Analysis of a proteome assembly obtained from the Ensembl Genomes server (Kersey *et al.*, 2012) yielded a set of 6902 APRs with TANGO scores greater than 5 (out of 100), which amounts to 2 APRs per bacterial protein on average. To reduce this to a manageable number, we selected the 25% APRs that have a TANGO score greater than 15, a threshold above which the false positive rate of TANGO is below 5% (see methods), and below 90 in order to exclude the most problematic sequences for peptide synthesis. To convert these APRs into aggregating peptides, we employed a design pattern based on a tandem of APRs flanked by arginine and lysine residues and separated by a glycine-serine linker, as shown in Supplementary Figure 1. The use of a tandem of APRs in our peptide design was motivated by the aim to generate relatively stable soluble oligomeric aggregates that have a strong potential to induce aggregation of target proteins (Benilova *et al.*, 2012). Such repeating patterns of aggregation prone segments are observed in naturally occuring amyloids that form stable soluble oligomers such as the yeast prion sup35 (Narayanan *et al.*, 2003), and the structural basis of the oligomer stabilisation by tandem repeats was recently revealed using x-ray crystallography (Laganowsky *et al.*, 2012). Finally, in order to improve synthesis efficiency and solubility this design template was supercharged by placing arginines at the flanks of the APRs. The charged residues act as aggregation gatekeepers that slow down beta-aggregation and increase colloidal stability by charge repulsion (Rousseau *et al.*, 2006b). As an additional benefit, the net positive charge of the peptides is expected to facilitate bacterial uptake (Hancock & Chapple, 1999, Torrent *et al.*, 2011). Peptides were generated by parallel micro-scale solid-phase synthesis, which yields peptide preparations of >80% purity for sequences below 20 amino acids without requiring HPLC purification.

Identification of bacterial APR peptide sequences with bactericidal activity

The conjunction of overall length limitation on peptide synthesis and with our tandem design pattern implied a restriction on the length of APRs of 5 to 7 amino acids, which yielded 263 suitable APRs in the *S. epidermidis* proteome, derived from 240 proteins (Supplementary Table 1). We determined the minimum inhibitory concentration (MIC) of these peptides on *S. epidermidis* ATCC12228. We found that 4 had low MIC values (1.5 - 6.0 $\mu g.mL^{-1}$, fig. 1A), *i.e.* peptide C29 (RLFNFLKRGSRLFNFLKR), C30 (RILLGLIRRGSRILLGLIRR), Hit1 (RWVSMLLRRGSRWVSMLLRR) and Hit50 (RFFIALSRRGSRVQAYLYRR). These hits were confirmed using HPLC purified material (>95%), which was used for all subsequent work. Interestingly, about 80% of the peptides generated using this design pattern are classified as antimicrobial peptides using the AMP prediction software CAMP (Waghu *et al.*, 2014), whereas only a small selection displayed actual antibacterial activity. On the other hand, 16% of a set of 2154 known antimicrobial peptides (Wang *et al.*, 2009) analysed displayed an APR meeting the TANGO threshold used here, and only 0.8% (17 cases) contained two APRs. This suggests that although there is a clear overlap between antimicrobial activity and aggregation propensity, the peptides analysed here differ significantly in structure and sequence compositions from known AMPs. Filtration of freshly dissolved samples using a 0.22 μm device had negligible effect on the apparent MIC value, indicating that very large particles do not contribute to activity, so we included this step in our standard sample preparation. The Minimum Bactericidal Concentration (MBC) of the four aggregating peptides was very similar to their respective MIC values (Figure 1A), demonstrating the bactericidal nature of these peptides.

We also analysed the activity against Staphylococcal strains with known antibiotic resistance. We found very similar MIC values for strains that were resistant to β-lactams via mecA expression (Chambers, 2001), strains resistant to glycopeptides (Pootoolal *et al.*, 2002) (supplementary Table 2), but also for *S. aureus* strain S113, that was shown to be resistant to known antimicrobial peptides such as defensins and cationic antimicrobial peptides (AMPs) via L-lysine surface modifications of the anionic membrane lipids (Kristian *et al.*, 2003, Peschel *et al.*, 2001). Finally, we evaluated the ability of the Methicillin resistant *S. aureus* strain 326 to develop resistance to C30 by repeated passaging and MIC

determination (Figure 1B). Continuous exposure to peptide C30 at 50% of its MIC concentration resulted in a transient two-fold increase in MIC that was lost again during further passaging. Similar results were obtained with the other peptides (Figure 1B). When MIC evolution was monitored over a longer period of time (31 instead of 15 days), no further increase in the MIC value was observed (Figure 1C). Compared to the common antibiotics, we observed a much slower onset of resistance development for both C30 and C29 than ampicillin, and smaller MIC value increases than for gentamicin and ampicillin (Figure 1B&C). Together these data demonstrate the antibiotic activity of these aggregating peptides.

Sequence specificity of bactericidal activity

Our aggregating peptides had much higher antimicrobial activity against *S. epidermidis* than against *E. coli* (Supplementary Table 3), which could possibly result from the differences in cell wall composition between Gram positive and –negative strains. However, scrambled versions of these peptides were much less active both against *S. epidermidis* and *E. coli*, even though they also aggregated (Figure 1A & Supplementary Figure 2), suggesting the antibacterial activity has a sequence-specific component. To further investigate the contribution of sequence information to peptide activity we determined the activity spectrum of the peptides against a wide range of bacterial strains (Supplementary Table 3). We then analysed how sensitivity correlated with the sequence conservation of potential target proteins. It is known that cross-seeding is most efficient between identical sequences (Ganesan *et al.*, 2014, Morales *et al.*, 2013), but that it is tolerant to some mismatches as e.g. in the co-aggregation between p53 and its homologs p63 and p73 (Xu *et al.*, 2011) or between the Alzheimer β-peptide and α-synuclein (Ono *et al.*, 2012). Therefore we considered as putative targets not only the proteins from which the APRs were taken but also proteins containing identical APRs or APRs that differed by a single amino acid substitution. To quantify the relationship between sequence conservation and peptide activity we evaluated the classification performance between sensitive and insensitive bacterial strains of different sequence conservation parameters using Receiver-Operator curve analysis (Figure 1D). These parameters included the number of

times the target APR sequence occurs in the entire genome, the conservation of the APR region in presumed target proteins and the overall sequence conservation of presumed target proteins. Gene expression levels or protein abundance counts could not be taken into account due to lack of data. As a consequence a significant level of false positives will handicap our analysis. Even so, non-mitigated genomic sequence information only allows predicting strain sensitivity reasonably well (Figure 1D). The presence of conserved APRs in homologous proteins seems to be a good predictor for cross-strain sensitivity (Figure 1D & Supplementary Table 3). For instance, using only the closest common putative target in sequence space as activity predictor (i.e. ClpC for C30, Glutamate-tRNA synthase for C29, Ribosomal Protein L10 for Hit1 and SugE Drug Efflux pump protein for Hit50) results in a Matthews Correlation Coefficient of 0.62 and an Area Under the Curve of 0.84 (Supplementary Table 3 & Figure 1D). This does not mean that activity is necessarily determined only by the closest common target protein and that additional and strain-specific proteins cannot also contribute to and modulate peptide activity. A scenario involving multiple targets would be in agreement with the slow buildup of antibiotic resistance against these peptides (Figure 1B&C). Additionally the variation in time-kill curves (Figure 1E) of the different peptides also suggests that other factors (such as differences in bacterial membranes and peptide uptake) also likely contribute to antimicrobial efficacy. Together, both the effect of scrambled peptides and the bioinformatics analysis above show that bactericidal peptide activity has a substantial sequence specific component. The question remains whether peptide activity is mediated through peptide-induced aggregation of bacterial proteins.

Bactericidal peptides form peptide aggregates

As expected from the design, we found the peptides to be highly aggregation-prone, forming aggregates that range from amyloid-like to an amorphous morphology by Transmission Electron Microscopy (TEM – Figure 2A and supplementary figure 2), depending on the sequence. After filtration with a 0,22 µm filter the size distribution in solution was determined by Dynamic Light Scattering (DLS) and ranged from monomers to oligomers up to 100 nm upon

dissolving to about 1 μm after several hours (50 μM in 50 mM PBS, Figure 2B). Ultracentrifugation of 200 μM peptide solutions (50mM PBS) at 250.000g for 140 min resulted in the precipitation of up to 30% of the material and by DLS the supernatant still contained both monomers and small oligomeric species. This shows that upon solubilisation the peptides most likely exist as a mixture of monomers and small soluble oligomers that that slowly convert to larger aggregates over a period of hours. To further probe the nature of the aggregates we performed tinctorial assays, in which the samples are analyzed in the presence of reporter dyes of which the fluorescence emission specifically changes upon interaction with beta-aggregates. For this purpose we used Thioflavin-T (ThT), a rotor dye that is well established for detecting amyloid structure (Sabate & Saupe, 2007), as well luminescence-coupled oligothiophene dyes (LCO) (Klingstedt et al., 2011, Hammarstrom et al., 2010, Aslund et al., 2009) which are a more recently developed but extensively validated family of amyloid sensor dyes with improved signal-to-noise ratio. In particular, we used pentameric oligothiophenes called p-HTMI and p-FTAA, which are similar in molecular structure but have opposite net charge. The peptides showed interaction with both LCOs tested as well as ThT from the earliest time points, although the intensity varied between the peptides and increased over time (Supplementary Figure 3C). Next, we analysed the secondary structure content of peptide samples using both Circular Dichroism (CD, Figure 2C) and Fourier Transform Infrared spectroscopy (FTIR, Figure 2D). The FTIR spectrum of our peptides is consistent with a mixed spectrum, composed of the double peaks at 1630 and 1680 cm^{-1} indicative of β-structure and a peak around 1655 cm-1, which is usually assigned to α-helix or random coil, e.g. the case of silk fibroin (Venyaminov & Kalnin, 1990). A mixed spectrum composed of both β-structure and random coil was confirmed by CD, with all peptides displaying a positive peak around 190 nm, in combination with a minimum around 200 nm and another dip around 220 nm (Rousseau *et al.*, 2006a). Taken together, these data confirm that upon solubilisation these peptides rapidly form complex mixtures, ranging from monomers to soluble oligomers by a mechanism of β-structure assembly that slowly matures into larger insoluble aggregates.

Peptides are internalized by bacteria but are not lytic

The intended mode of action of these aggregating peptides requires the ability to induce the aggregation of intracellular bacterial proteins. As this implies the ability of the peptides to be internalized, we investigated peptide localization by transmission electron microscopy (TEM). In particular, we have exposed Methicillin resistant S. aureus strain 326 to FITC labelled peptides and revealed their location using immunogold labelled anti-FITC antibodies in thin sections of bacterial pellets, which showed clear accumulation of peptides inside bacteria (Supplementary Figure 5A). In contrast to well-known lytic antimicrobial peptides (Last & Miranker, 2013), peptide internalization is not associated with obvious defects of cell membrane structure or cell morphology within a 30 min time lapse. The ultrathin section of bacteria showed intact membranes without inner pores or obvious perturbations commonly observed with detergent-acting or carpet-like AMPs (Yeaman & Yount, 2003) (Supplementary Figure 5A). Further, contrary to what is observed upon treatment with cationic α-helical and amphiphilic antimicrobial peptides (Anderson *et al.*, 2004, Li *et al.*, 2014, Hartmann *et al.*, 2010), no significant cytoplasmic leakage from the membrane could be observed (Supplementary Figure 5A). Scanning electron microscopy (SEM) revealed small cell wall irregularities (previously defined as blebs or craters(Hartmann *et al.*, 2010)) after 15 min that became more obvious and were accompanied by a small (10%) reduction of the cell diameter after 30 min and 1 h (Supplementary Figure 5B & 6A). The shrinkage is consistent with the finding that well-folded or aggregated proteins occupy less cytoplasmic space and that cell-volume regulation is affected directly by macromolecular crowding (Boersma *et al.*, 2015). The structures observed via SEM are not comparable to pores formed by AMPs such as melittin or cecropin (Brogden, 2005). Moreover, it was shown for several AMPs that a transmembrane potential is required for pore formation, both in intact cells and in artificial bilayers and that depolarisation of the membrane, e.g. using the chemical carbonyl cyanide rn-chlorophenylhydrazone (CCCP) prevents pore formation (Schuller *et al.*, 1989). However, pre-treatment of bacteria with CCCP had no effect on the bactericidal effect of our peptides (Supplementary Figure 6B). Together these data suggest peptide internalization occurs without immediate and severe disruption of the

cell wall and cell membrane and suggests that the bactericidal activity of these peptides is not primarily due to membrane-perturbing effects.

Peptides induce intracellular aggregation in bacteria

The most striking morphological change observable upon peptide treatment consisted of a clearly disturbed process of cell division. Division of peptide-treated cells was asymmetrical when compared with untreated staphylococci; septa also were much thicker and lost their margin (Supplementary Figure 5A). Interestingly, in conjunction aggregate clusters could be seen only in one part of the cell, reminiscent of asymmetric segregation heritance of aggregates, a process described previously in *E. coli* (Rokney et al., 2009, Lindner et al., 2008). In order to study the relationship between cell death and aggregation we performed two-dimensional flow cytometry whereby we quantified cell death by propidium iodide (PI) staining in one channel and aggregation in the other channel using p-FTAA, a luminescence-coupled oligothiophene dye which was previously shown to display characteristic changes in its fluorescence spectrum upon interaction with amyloid-like aggregates *in vitro* as well as *in vivo*. After treatment with our peptides, the bacteria showed a clear increase in staining for both dyes suggesting a tight association between bacterial death and protein aggregation (Figure 3A & B). In contrast, treatment with scrambled versions of the peptides resulted in increased p-FTAA staining but not in increased PI staining except for scrambled C30 that is still partially active (Figure 3C).

In order to differentiate between the accumulation of aggregated peptide inside bacteria and intracellular peptide-induced protein aggregation, we proceeded to carry out aggregation assays in combination with mass spectrometry in order to characterize changes in protein levels in the soluble and insoluble fraction after treatment of Methicillin resistant S. aureus strain 326 with C30, C29 and Hit1 in comparison to untreated controls (Supplementary Table 4 & 5). We could identify 66 unique proteins that increase in the insoluble fraction upon peptide treatment (Figure 3D), of which 50 (76%) are uniquely enriched in response to treatment with one of the peptides, indicating each peptide affects the solubility of a specific set of proteins within the bacterial proteome. On the other hand four proteins (6%) are commonly found in the aggregated fraction of all peptide

treatments, and the remaining 12 (18%) are found to aggregate with at least two peptide treatments. The four proteins that commonly aggregate with all three peptides tested are 50S ribosomal protein L5 (RplE), Alkaline shock protein 23, Putative transaldolase and Alkyl hydroperoxide reductase subunit C, of which only the RplE protein is essential for bacterial viability (Chaudhuri *et al.*, 2009). Gene Ontology term enrichment analysis using the NCBI David server (Huang da *et al.*, 2007) shows that the largest enriched group of genes is those associated with translation, including many ribosomal components (31% of the set, Benjamini correct p-value of 10^{-21}). Three molecular chaperones Trigger Factor, GroEL, DnaK and the protease ClpX are also detected, in line with an aggregation-associated mode of action. The closest putative target proteins in sequence space are detected but only the presumed C29 target Glu-tRNA synthase is significantly enriched in the aggregated fraction, for Hit1 a three-fold enrichment of the presumed target is detected, but does not pass the statistical testing whereas for ClpC, the presumed target of C30, we find an overall reduction of the protein in both fractions. Together these data demonstrate that peptide treatment results in intracellular protein aggregation. Our data also indicate that the aggregated proteome is peptide-specific and confirm that bacterial cell death and protein aggregation are associated phenomena. However, these data fall short of delivering clear evidence that peptides indeed interact with homologous sequences in endogeneous bacterial proteins, and thus inducing aggregation of bacterial proteins in a peptide-specific manner

Aggregating peptides are toxic to bacteria but not to mammalian cells

Since S. aureus is able to grow inside human cells, e.g. during a gut infection, we determined the ability of our aggregating peptides to protect the mammalian cells from staphylococcal infection and kill intracellular bacteria. To this end we inoculated cultures of human HCT116 cells with 0.5 x 10^5 CFU of the *S. aureus* strain 326, resulting in bacterial growth inside the mammalian cells. Treatment with a fluorescent derivative (Dylight488) of peptide C30 or Hit50 revealed specific accumulation of the peptides in the bacterial cells (Figure 4A-B). Peptide accumulation in the bacteria co-stained with propidium iodide (PI), a dye that selectively labels dead cells, demonstrating the bactericidal effect of the peptides

inside the mammalian cells (Pearson's correlation coefficient 0.41 and overlap score 0.94). The images obtained by confocal microscopy show that the aggregating peptides can selectively kill bacteria both extra- and intracellularly, helping in full clearance of invasive staphylococcal infection. Moreover after 72 h of infection, cells treated with peptides showed full recovery to a healthy cell monolayer (Figure 4C). To quantify intracellular bactericidal efficacy of aggregating peptides, a microtitre plate screening assay for bacterial invasion was used (Nizet *et al.*, 1998). In brief, a HCT116 cell monolayer was infected with Methicillin resistant S. aureus strain 326, washed to remove extracellular bacteria and lysed to release intracellular bacteria. The CFU number of each treatment was determined and compared to that of untreated infected controls (Figure 4D). The test showed that all peptides decreased significantly the amount of bacteria residing in HCT116 cells (Anova, $p<0.05$, Bonferroni's Multiple Comparison Test), outperforming the vancomycin treatment (Supplementary figure 7).

To control for adverse effects on mammalian cells - in particular because lipid membrane disruption by amyloid-like aggregates has been described before (Evangelisti *et al.*, 2012) - we first determined the hemolytic activity of the peptides on human red blood cells. We monitored haemoglobin release via absorbance at 414 nm after peptide treatment (Figure 4E). The test showed little hemolysis at concentrations near the MIC values. The cytotoxic effect of peptides was studied on various mammalian cell lines, including human colon carcinoma cell line (HCT116, Figure 4 A & F), human embryonic kidney cell line (HEK293T, Supplementary Figure 8A) and mouse fibroblasts (NIH3T3, Supplementary Figure 8B) using both the Alamar Blue (Invitrogen) and WST-1 (Roche) colorimetric assays. For most peptides no significant cytotoxicity towards these mammalian cells was observed at concentrations up to 10 times above the MIC value of the peptides. At concentrations as high as 100 $\mu g.mL^{-1}$ (16 to 100 times the MIC, depending on the peptide) mammalian cells showed 80-100% recovery within 3-24 hours (Figure 4F and Supplementary Figure 8). These results further argue against a generic mode of action based on membrane disruption alone.

Aggregating peptides cure mice from bacterial sepsis

We determined the antibacterial activity of three peptides (C30, C29 and Hit50) in six-week-old, specific-pathogen free, inbred female BALB/cOlaHsd mice (20-23 g) in which sepsis was induced by intravenous inoculation of 150 µL of a bacterial suspension containing 8.10^9 CFU.mL^{-1} of MRSA strain 326. Treated mice received a single dose of aggregating peptide 30 min post bacterial inoculation at 15 mg.kg^{-1} for C30 and 10 mg.kg^{-1} for C29 and Hit50. One control group received the antibiotic vancomycin at 15 mg.kg^{-1} and the other control group received mock injections. Survival was monitored in all groups until the untreated group dropped below 20% survival, which took between 3 and 5 days (Figure 4G). The analysis of survival percentage revealed a clear and statistically significant protective effect of the treatment with aggregating peptides (analyzed using the log-rank test via Prism 4 software). Mice rescued from sepsis using our aggregating peptides and vancomycin appeared to make full recovery to normal health and were sacrificed six months after the experiment and samples from all major organs were analyzed histologically (Supplementary Table 6). The analysis revealed no major abnormalities in the peptide-treated animal compared to the vancomycin-treated controls and revealed mainly scarring caused by the bacterial sepsis.

The dose of peptide used for treatment was determined in a separate 5-day dose-escalation experiment in uninfected animals, (3 mg.kg^{-1} on day one and 6, 12.5, 15 and 30 mg.kg^{-1} on subsequent days). Overall, we observed few adverse effects of peptide treatment, except at the highest dose when general lethargy was observed. After day 5, animals were sacrificed and histological staining of heart, kidney, liver and spleen (Supplementary Figure 9) as well as a full hematological analysis (Supplementary Table 7) was performed. These showed no major abnormalities in the treated animals apart from a minor increase in the number of peripheral neutrophils and possibly a slight hemolytic effect. This increase in the number of peripheral neutrophils may be related to a generic capacity of amyloid fibrils to elicit neutrophil extracellular trap secretion (Azevedo *et al.*, 2012).

Discussion

The need for new antibiotics is generally acknowledged. Yet screening for naturally occurring molecules, still the source of the majority of drugs in clinical use today, has been largely abandoned as the yield of novel compounds dropped and genomics, *in silico* drug design and targeted screening of compound libraries have not delivered the much hoped-for new targets (Livermore, 2011). We here explored the possibility to target the well-known toxic potential of protein aggregation to specific microorganisms using bacterial aggregation prone sequences, whilst minimally affecting their host as a way to open novel avenues to fight infectious diseases. As most bacterial proteins contain aggregation prone sequences, the potential to exploit aggregation as a bactericidal mechanism opens a rich chemical space that remains to be explored. However, it is clear that before this exciting novel mode of action can be employed in a therapeutic setting, significant improvements of the peptides need be achieved and their modes of action to be better understood. Most importantly, the exact chain of events leading from aggregation to rapid cell death remains to be fully elucidated.

Our design paradigm generates aggregation-prone peptides and bacteria spontaneously internalize the active aggregating peptides with minimal apparent disruption of the cell membrane, similar to the penetration of aggregated mammalian proteins into mammalian cells (Ren *et al.*, 2009, Munch *et al.*, 2011) or non-lytic AMPs. Upon peptide uptake we observe aggregation of bacterial proteins in association with cell death. We showed that among the active peptides from an unbiased screen of hundreds of APRs, only a small set of sequences displays antimicrobial activity, while all share a high hydrophobicity and net positive charge. This suggests that aggregate toxicity is sequence-dependent but also that additional factors are probably required to confer aggregate toxicity. The aggregated proteins detected in treated bacteria were specific to the peptide used, strongly suggesting each peptide triggers the aggregation of particular proteins. Sequence analysis of the activity profile of the peptides towards various bacterial strains shows that homology between the aggregation prone region of the peptide and the target protein predicts activity to some extent, but clearly indicates that other factors also play a role. Hence, although our results are consistent with the intended mode of action involving

the homologous seeding of aggregation by synthetic peptides based on the aggregation prone sequences of a protein of the target species, our current data come short of delivering the ultimate evidence that this is the case. It also remains unclear how this initial event leads to widespread aggregation and eventually lethal proteostatic collapse.

The very rapid bactericidal effect on the other hand is not commonly observed in currently used antibiotics that interact with similar targets and may indicate a direct toxic effect of the aggregates. They directly perturb essential cellular processes by sequestration of newly synthesised protein (Olzscha *et al.*, 2011) or by the disruption of cellular membranes (Lashuel & Lansbury, 2006). Factors that play an additional role may include sequence-dependent uptake efficiency (Aguzzi & Rajendran, 2009) or aggregate size (Shankar *et al.*, 2008, Lesne *et al.*, 2006) and conformation (Campioni *et al.*, 2010, Laganowsky *et al.*, 2012). In support of this, bacterial intracellular aggregates have been shown to induce oxidative stress, including production of free radicals resulting in damage to other cellular proteins. The mass spectrometry results suggest that the proteolytic machinery of the cell is involved and may become overloaded. Due to aggregation and constant synthesis of new proteins, the cytoplasm becomes a crowded environment, allowing the co-aggregation of newly synthesized proteins and proteins with exposed aggregation prone-regions. This cascade may in turn lead to lipid peroxidation and membrane lipid rearrangements, which result in over expression of membrane proteins, porins, toll-like receptors and ion pumps (Bednarska *et al.*, 2013, Spitzer & Poolman, 2013).

In the homologous seeding model, it easy to imagine why the peptides do not similarly affect mammalian cells as presumably the heterologous seeding of the aggregation of host proteins is much less efficient due to the diversity in amino acid sequence and protein structure, possibly amplified by difference in cellular uptake efficiency. However, during the screening process presented here, we did not filter out sequences with matches in the human proteome and indeed, homologous sequences can be found in human although we did not detect aggregation or toxicity to mammalian cells either *in vitro* or *in vivo*. We can only speculate as to why bacterial cells are more sensitive than mammalian cells to aggregating peptides and future research should undoubtedly be

dedicated to clarifying these issues. Differences could reside in differences in cell size and rate of metabolism of bacteria and mammalian cells: the smaller size of bacteria as well as their higher metabolism which poses higher demands on the proteostatic machinery of the cell could both explain a lower resistance to proteostatic collapse. Differential peptide uptake efficiency could be another factor contributing to differences in sensitivity to aggregation.

Protein-specific factors could also explain differences in susceptibility. First, all potential target proteins are not necessary expressed or sufficiently highly expressed. Second, APR susceptibility will also be affected by the structural context and thermodynamic stability of target proteins: APRs that are surface exposed will be more easily targeted than structurally protected APRs and thermodynamically unstable proteins will be more readily prone to aggregation than more stable proteins. All these parameters might therefore further contribute to and modulate peptide efficacy and remain to be investigated in more detail.

It is of interest that the precise nature of other well-described AMP-membrane interactions is still unknown; nonetheless different mechanisms of membrane interaction have been proposed, including carpet-like, barrel-stave pore, toroidal pore and aggregate models (Shai, 2002, Matsuzaki, 1998, 2001, Wu *et al.*, 1999). Other data support the idea that peptides form local aggregates on the outer leaflet, pass through the membrane by a self-promoted uptake, reach and cross the cytoplasmic membrane and finally interact with polyanionic targets such as DNA and RNA (Hancock & Chapple, 1999). Although the mode of action usually involves disrupting the integrity of the bacterial cytoplasmic membrane, alternative antimicrobial mechanisms have been found and characterized. Antimicrobial peptides that target key intracellular processes, including DNA and protein synthesis, protein folding, enzymatic activity and cell wall synthesis have been described and lead to a new sub classification of AMPs as membrane disruptive and non-disruptive (Powers & Hancock, 2003). Regardless of whether the AMPs permeabilize the membrane or just flip through the membrane to reach the internal target, they all must interact with it. In general the activity of most AMPs on *S aureus* is much lower than against other Gram-positive bacteria. This is mostly due to the Staphylococcal membrane

composition of negatively charged lipids, such as phosphatidylglycerol and cardiolipin (Epand & Epand).

Experimental Procedures

Bioinformatics

We used the TANGO algorithm for all APR identifications in this manuscript. We used a cutoff on the TANGO score of 5 per residue since this gives a Matthews Correlation Coefficient between prediction and experiment of 0.92 (Fernandez-Escamilla *et al.*, 2004). The settings of TANGO were Temperature = 298, pH = 7.5, Ionic Strength = 0.10.

Bacterial strains and media

Organisms were grown in BHI (brain-heart infusion) media, subcultured and quantified in cation adjusted Muller-Hinton broth (CAMHB), Tryptic soy broth (TSB), tryptic soy agar (TSA) or blood agar (BA). Micro-organisms included Gram-positive *Staphylococcus aureus* type strain ATCC29213; clinical isolates of methicillin-resistant *S. aureus* (MRSA) (strains nr 204, 418, 274, 165, 351, 115, 651), *S. epidermidis* type strain ATCC13228; clinical isolates of methicillin-resistant S. epidermidis (MRSE) (strains nr 101, 103, 104, 109), clinical isolates of S. capitis*, S. hominis, S. haemolyticus, Enterococcus faecalis* type strain ATCC 19433: clinical isolates of vancomycin resistant *E. faecium* (VRE) (strains nr 8, 11, 12, 40, 60, 70, 54), other Gram-positive strains: *Nocardia asteroides* type strain ATCC 3308, *Micrococcus luteus* type strain ATCC 9341, *Listeria monocytogenes* type strain ATCC 11994, Bacillus subtilis type strain ATCC 6051, B. subtilis type strain IP 5832, clinical isolates of B. cereus (strains nr 1 and 2). Gram-negative isolates *Klebsiella pneumoniae* type strain ATCC13883, *Salmonella choleraesuis* type ATCC13311, *Escherichia coli* type strain ATCC25922, *Pseudomonas aeruginosa* type strain ATCC27853.

Peptides

During the screening stage peptides were synthesised using standard solid-phase peptide synthesis (JPT, Berlin, Germany). Peptide hits were resynthesised in-house at higher scale using an Intavis Multipep RSi synthesis robot and HPLC purified to 95% using Zorbax SB-C3 semi-preparative column (Agilent, USA) on a Prominence HPLC (Shimadzu, Japan). Peptides were lyophilized and stored at -20 °C prior to use. Stock solutions of each peptide were prepared in 50% DMSO

in ddH2O or for *in vivo* use in 25mM His-Acetate, 137mM NaCl + 12mM KCl + 1% Hydroxypropyl Beta Cyclodextrin buffer, pH 6.5. For biophysical and structural characterisation peptides were prepared in 25 mM Mes pH 6.5.

Primary screening of peptide libraries, minimum inhibitory concentrations (MIC) and minimum bactericidal concentrations (MBC)

The microbroth dilution method with two-fold serial dilutions in CAMHB (according to EUCAST guidelines) was used for routine screen of peptide libraries, with concentrations ranging from 0.3μg.mL^{-1} to 200μg.mL^{-1}. Bacteria were grown in a shaking incubator at 37°C and 160 rpm in 50 mL BHI , using individual colonies retrieved from a fresh overnight TSA-sheep blood plate. Cultures were grown to a density of approximately 1x10^{8} CFU.mL^{-1} and then diluted to 5x10^{5} CFU.mL^{-1} in CAMHB (Mc Farland 0.5). Each well contained 100 μL (50 μL of peptide containing MHB plus 50 μL inoculum). The final cell density was 1x10^{5} to 5x10^{5} CFU.mL^{-1}. Controls on each plate included a blank medium control, a 100% growth control (medium + inoculum) and a DMSO-effect control (40 μL medium + 10 μL 50% DMSO + 50 μL inoculum). After addition of the cell suspension, plates were incubated at 37°C for 18 to 24 h. The optical density at 590 nm (OD590) of each well was measured after 5 s of shaking using a Perkin Elmer spectrophotometer (1420 Multilabel Counter Victor 3). Wells without growth were plated on TSA-sheep blood agar plates, incubated at 37°C overnight and visually inspected. MBCs were defined as the minimum concentration of agent that brought about >99.9% killing of the organism.

Biophysical characterization

Dynamic light scattering (DLS) measurements were made at room temperature with a DynaPro DLS plate reader instrument (Wyatt, Santa Barbara, CA, USA) equipped with a 830-nm laser source. Samples (100 μL PBS buffer, 2 mM peptide) were placed into a flat-bottom 96-well microclear plate (Greiner, Frickenhausen, Germany). The autocorrelation of scattered light intensity at a 90° angle was recorded for 10 s and averaged over 40 recordings to obtain a single data point. The Wyatt Dynamics software was used to calculate the hydrodynamic radius by assuming a spherical particle shape. Attenuated Total

Reflection Fourier Transform Infrared Spectroscopy (ATR FTIR) was performed using a Bruker Tensor 27 infrared spectrophotometer equipped with a Bio-ATR II accessory. Spectra were recorded in the range of 900 –3500 cm-1 at a spectral resolution of 4 cm-1 by accumulating 120 data acquisitions. The spectrophotometer was continuously purged with dried air. Spectra were corrected for atmospheric interference, baseline-subtracted, and rescaled in the amide II area (1500 to 1600 cm-1). For Transmission Electron Microscopy (TEM) aliquots from peptide preparations were adsorbed to carbon-coated Formvar 400-mesh copper grids (Agar Scientific) for 1 min. The grids were blotted, washed, and stained with 1% (wt.vol^{-1}) uranyl acetate. Samples were studied with a JEOL JEM-1400 microscope (JEOL Tokyo, Japan) at 80 kV.

Hemolysis assay

Serial twofold dilutions of the compounds were prepared in Tris Histidine-Acetate buffer (pH 7.0) and distributed in 96-well plates. Fresh human red blood cells (RBC) from peripheral blood were obtained by centrifuging at 1,000 x g, washed in PBS (pH 7) and resuspended in PBS to a final concentration of 10% v/v. The RBC suspension (200 µL) was added to each well, and the following controls were included: PBS only, physiological water, 0.1% Tween X-100, histidine-acetate buffer. The plate was incubated at 37°C for 1 h. Following centrifugation at 1000 x g, supernatant was aspired carefully by pipette and transferred to a fresh 96-well plate. Hemolysis was assessed by measuring the absorbance at 414 nm and calculated as the percentage of total hemolysis, defined as hemolysis induced by 0.1%Tween X-100.

Alamar Blue assay

Cellular toxicity was measured by the Alamar Blue (AB) conversion assay, based on resazurin as an active agent, which changes color and becomes highly fluorescent upon conversion to resorufin, which is directly associated with reducing power of living cells. A subconfluent monolayer culture of human embryonic kidney cells (HEK293T), human colon carcinoma (HCT116) or mouse embryonic fibroblasts cell line (NIH3T3) were trypsinized (0.5%-EDTA Trypsin, Gibco, Invitrogen) and diluted in Dulbecco's Modified Eagle Medium (GIBCO®

DMEM Media, Invitrogen) to contain $3x10^3$ cells.mL^{-1}, and 50µL of this mixture was aliquoted into 96-well plates and allowed to incubate at 37°C in the presence of 5% CO2. At the same time, separate 96-well plates with different concentrations of peptides (final volume 50 µL) were prepared by twofold serial dilutions in DMEM medium, and pre-warmed in a 37°C incubator prior to adding to the cell-containing test plate. The cells with the added peptide mixtures were incubated for 2, and 24 h. After incubation, 50µL of AB reagent was added and incubation was continued for another 2-4 h. Appropriate controls were included, namely: untreated cells, lysed cells (using lysing reagent for the LDH-release kit, Roche), DMSO treated cells, buffer + peptide + AB reagent only control. Both the fluorescence (excitation 530 nm, emission 590 nm) and absorbance (570 nm, using 600 nm as a reference wavelength) were measured. Percentage of viability was calculated as follows: (Mean of test value-negative control value)/ (positive control value-negative control value)*100. The amount of fluorescence produced is proportional to the number of living cells.

Invasion assay

In this assay, mammalian cell monolayers (human colon tumor cell line HCT116 or human embryonic kidney cell line HEK293T) were cultured at the bottom of a microwell plate. The next day 50µl of fresh S. aureus MRSA strain 326 were added (approximately 10^6 CFU.mL^{-1}) and a negative uninfected control included. After 90 min of infection different concentrations of peptides were added and the cell cultures were incubated for another hour. As a positive control, gentamicin was used. Each well was washed with pre-warmed physiological water to remove any extra-cellular bacteria, followed by 1% Triton treatment to release all intracellular bacteria from the mammalian cells. The content of the well was serially diluted and plated on TSA agar plates for CFU count.

Fluorescence microscopy of co-cultures

For imaging purposes, human HCT116 colon carcinoma cells were grown to form a confluent monolayer, infected with 50 µl (10^6 CFU.mL^{-1}) of *S. aureus* MRSA strain 326 for 48 h. The monolayer was treated with DyLight488-tagged peptide at its MIC. Cells were stained with CellMask plasma membrane stain and

Propidium Iodide (Invitrogen), and images taken with a Zeiss CLSM 510 Meta NLO confocal microscope after 1 h of peptide-treatment. To monitor recovery of infected cells, the medium was replaced and supplemented with peptides, and the confluence of the monolayer was inspected after 72 h.

Flow cytometry analysis of bacteria using aggregation-specific luminescent conjugated oligomers (LCOs)

Exponential growth phase *S. aureus* MRSA strain 326 cells were washed in PBS, aliquoted into FACs tubes, treated with peptides at 2 x MIC. At specific time points, cells were incubated with a mixture of the LCO dye p-FTAA (450/507) and Propidium iodide (PI, 535/617). To correlate the aggregation with cell death, the fluorescence intensity was measured in two channels using a flow cytometer (Canto, BD Biosciences). Penicillin-, vancomycin-, novobiocin- treated and untreated and unstained cells were used as controls.

Scanning electron microscopy

Bacteria of mid-exponential growth phase were diluted with salt free medium to a density of 10^6 CFU.mL^{-1} and treated with supra-MICs of peptides. After 5, 30 and 60 min the bacteria were fixed with 2.5% glutaraldehyde in 0.05 M NaCacodylate buffer (pre-warmed to 37°C). Cells were pelleted and resuspended in the same buffer and incubated for 45 min at room temperature. Samples were washed in 0.05 Na-Cacodylate buffer repeatedly and post-fixed with 1% Osmium tetroxide. The samples were dehydrated with a graded ethanol series (50%, 70%, 96%, 100% of alcohol). After the last step of dehydration, hexamethyldisilazane was added and incubation continued for 45 min. The sample was loaded on a supporting stub for SEM, covered with a thin layer or platinum (Agar Auto Sputter Coater) to avoid charging in the microscope. Microscopy was performed using a JEOL 7401F scanning electron microscope.

Transmission electron microscopy on ultrathin sections

Exponential phase bacteria were treated with different supra-MICs of peptides for 20 min. After the treatment, cells were progressively fixed with Karnovsky fixative (2% paraformaldehyde + 2,5% glutaraldehyde in 0,1 M cacodylate

buffer). After 10 washing steps in cacodylate buffer, the cells were embedded in 2% Noble agar (Difco), centrifuged to get an even pellet, cooled down and cut into small cubes. Samples were then postfixed in 1% buffered osmium tetroxide for 1h, stained en block with 1% uranyl acetate, dehydrated in a graded series of ethanol and embedded in Agar 100 (Epon epoxy resin, Miller-Stephenson). Thin and ultra-thin sections were prepared on carbon-stabilized copper grids and stained with 1% uranyl acetate and lead citrate. Samples were observed using a JEOL JEM 2100 Transmission electron microscope operating at accelerating voltages of 80kV and 200kV.

Immuno-electron microscopy

Bacteria in the exponential growth phase were treated with FITC-tagged peptide (at 2 x MIC value) for 30 min followed by fixing with double strength fixative (4% paraformaldehyde + 0.4% glutaraldehyde in 0.1M cacodylate buffer, pH=7.4) for 10 min and single strength fixative (half of above) for 1 h. After several washing steps (cacodylate buffer and cacodylate /glycin buffer) the pellet was suspended in 12% gelatin/cacodylate-buffer, incubated on ice, cut in small cubes and set to incubate overnight in 2.3 M sucrose. Samples were mounted on specimen holders, frozen in liquid nitrogen, and sectioned with a Diatome cryo diamond knife at -100°C with a Leica ultracut UCT with EMFCS cryokit. Ultrathin thawed sections were placed on Formvar-carbon-coated copper grids (400mesh). Grids were then washed in 50 mM PBS buffer for 5 min, blocked with PBS/BSA (0.1%) and incubated for 30 min in a drop of anti-FITC goat primary antibody (Abcam) (diluted 1:1000 in PBS/BSA 1% buffer), washed 5 times in PBS/BSA 0.1% buffer, incubated for 30 min with rabbit anti-goat protein-A-gold conjugate (5nm; BBInternational EM Rag5) and diluted 1:50 in PBS/BSA 1% buffer. The sections were then washed 6 times for 5 min in PBS and 3 times in ddH2O. Grids were stained for 5 min with 0.4% uranyl acetate – 1.8% methyl cellulose on ice, looped out and blotted so as to obtain an even thin layer only encasing the sections, and observed using a JEOL JEM 2100 Transmission electron microscope, operated at an accelerating voltage of 80kV.

In vivo experiments

Animals: Six-week-old, specific-pathogen-free, NIH Swiss female mice (Harlan Sprague-Dawley, Indianapolis, IN) weighing 20 to 23 g were used for all studies. All experimental procedures were approved by the local Animal Ethical Committee. To determine the maximum tolerated dose in the mouse, compounds were prepared in sterile 25mM His-Acetate, 137mM NaCl + 12mM KCl + 1% Hydroxypropyl Beta Cyclodextrin buffer, pH 6.5. Mice were treated with compounds injected intravenously (i.v.). Injections were given once a day over a 5 day period via the tail vein, starting from a dose of 3 $mg.kg^{-1}$ and escalating to 6, 12.5, 15 and 30 $mg.kg^{-1}$. The following signs were recorded: reduced motor activity, pilo-erection, redness in the ear lobe, cyanosis, protruding eyeballs, slow or labored breathing, los of response in the rear legs, convulsions, and death. After 5 days of treatment, blood was sampled through retro orbital puncture from each animal and analyzed. For the long-term side-effects, remaining animals were kept under day-to-day observation over a period of 7 days after the last treatment, sacrificed and organs subjected to histological analysis. Organs and tissues collected for microscopical evaluation were fixed in 4% PFA, embedded in paraffin, sectioned and stained with hematoxylin and eosin using standard methodologies.

Sepsis mouse model of infection: 100 µL of solution containing approximately 8 x 10^9 $CFU.mL^{-1}$ S. aureus MRSA clinical strain 326 was injected i.v.. Mice were treated 30 min post-infection with half of the maximum tolerated dose of peptide. Vancomycin at the same concentration was used as a control for 100% survival and an untreated mice group was used as a 100% lethality of the infection control. The endpoint was determined at 72h-120h post-infection, depending upon the untreated group survival dropping below 20%.

Mass Spectrometry Experiments

Following incubation with aggregating peptides for 60 min, bacteria were lysed in PBS using a French press. The resulting lysate was centrifuged for 10 min at 4000 rpm at 4°C to obtain a soluble (supernatant) and an insoluble (pellet) fraction. The pellet was then washed 3 times in phosphate buffered saline. For the label-free experiment, both fractions were dissolved in sample loading buffer

and separated briefly by SDS-PAGE. The protein band was stained with SimpleBlue (Thermo), excised and in-gel digested using trypsin.

The obtained peptide mixtures were introduced into the LC-MS/MS LTQ-Orbitrap Velos system using a tandem configured(Mitulovic *et al.*, 2009) Ultimate 3000 RSLC nano LC (Thermo Scientific, Bremen, Germany) in-line connected to an LTQ-Orbitrap Velos (Thermo Fisher Scientific). The sample mixture was first loaded on a trapping column (made in-house, 100 μm I.D. x 20 mm, 5 μm beads C18 Reprosil-HD, Dr. Maisch, Ammerbuch-Entringen, Germany). After flushing from the trapping column, the sample was loaded on an analytical column (made in-house, 75 μm I.D. x 150 mm, 5 μm beads C18 Reprosil-HD, Dr. Maisch). Peptides were loaded with loading solvent A (0.1% trifluoroacetic acid in water/acetonitrile, 98/2 (v/v)) and separated using a linear gradient from 2% of solvent A' (0.1% formic acid in water) to 50% of solvent B' (0.1% formic acid in water/acetonitrile, 20/80 (v/v)) at a flow rate of 300 $nl.min^{-1}$ followed by a wash reaching 99% of solvent B'.

The mass spectrometer operated in data-dependent mode, automatically switching between MS and MS/MS acquisition for the ten most abundant peaks in a given MS spectrum. In the LTQ-Orbitrap Velos, full scan MS spectra were acquired in the Orbitrap at a target value of 1E6 with a resolution of 60,000. The ten most intense ions were then isolated in the linear ion trap with a target value of 1E4, with a dynamic exclusion of 60 s, and fragmented. For data processing, the following Mascot workflow was used. From the MS/MS data in each LC run, Mascot Generic Files were created using the Distiller software (version 2.4.3.3, Matrix Science, London, UK, http://www.matrixscience.com/distiller.html). These peak lists were then searched with the Mascot search engine (Matrix Science) using the Mascot Daemon interface (version 2.4.0, Matrix Science). Spectra were searched against the *Staphylococcus aureus* MRSA database extracted from NCBI on 18/11/2013 containing 6,404 protein sequence entries. Variable modifications were set to pyro-glutamate formation of amino-terminal glutamine, formylation of the protein N-terminus, oxidation of methionine and C-propionamide modification of cysteine side-chains. Mass tolerance on peptide ions was set to ±10 ppm (with Mascot's C13 option set to 1), and the mass tolerance on peptide fragment ions was set to ±0.5 Dalton (Da). The peptide

charge was set to 1+,2+,3+ and instrument setting was put on ESI-TRAP. The enzyme setting was trypsin allowing for one missed cleavage, and cleavage was allowed when arginine or lysine were followed by proline. Only peptides that were ranked first and scored above the threshold score, set at 99% confidence, were withheld. All data was processed and managed by ms_lims(Helsens *et al.*, 2010).

False discovery rates were calculated according to Käll *et al(Kall et al., 2008)*. and were on average 0.05% for the label free experiments.

Label-free quantitation

By using the percentage of the spectral count, the portion of the protein present compared to the complete set of proteins present can be calculated. Next, the fold change can be calculated of the portion of a protein present in the soluble fraction compared to the insoluble fraction (supplementary table). By applying a Bonferoni correction and a t-test we show that some proteins are present in different amounts in the soluble and insoluble fraction.

Acknowledgements

The Switch Laboratory was supported by grants from VIB, University of Leuven, the Funds for Scientific Research Flanders (FWO), the Flanders Institute for Science and Technology (IWT) and the Federal Office for Scientific Affairs of Belgium (Belspo), IUAP P7/16. The Laboratory of Clinical Bacteriology and Mycology was supported by a grant from the Flanders Institute for Science and Technology (IWT). Per Hammarström and K. Peter R. Nilsson are supported by the Swedish Foundation for Strategic Research (K.P.R.N, PH) & the Swedish research council (P.H.). K.P.R.N is financed by an ERC Starting Independent Researcher Grant (Project: MUMID) from the European Research Council. We thank Dr Peschel for the kind donation of the *S. aureus* S113 and Delta mprF strains. We thank Dr Colin Bayne for valuable advise and experitise in proteomics approaches as well as Moredun Research Institute for 2D gel analysis training provided.

Conflict of Interest Statement

The host institution VIB has filed a patent application on behalf of the F.R. and J.S. describing the design concept of the peptides presented in this manuscript.

References

(2001) *(NAS Colloquium) Virulence and Defense in Host--Pathogen Interactions: Common Features Between Plants and Animals*. The National Academies Press.

Aguzzi, A. & L. Rajendran, (2009) The transcellular spread of cytosolic amyloids, prions, and prionoids. *Neuron* **64**: 783-790.

Anderson, R.C., R.G. Haverkamp & P.L. Yu, (2004) Investigation of morphological changes to Staphylococcus aureus induced by ovine-derived antimicrobial peptides using TEM and AFM. *FEMS Microbiol Lett* **240**: 105-110.

Aslund, A., C.J. Sigurdson, T. Klingstedt, S. Grathwohl, T. Bolmont, D.L. Dickstein, E. Glimsdal, S. Prokop, M. Lindgren, P. Konradsson, D.M. Holtzman, P.R. Hof, F.L. Heppner, S. Gandy, M. Jucker, A. Aguzzi, P. Hammarstrom & K.P. Nilsson, (2009) Novel pentameric thiophene derivatives for in vitro and in vivo optical imaging of a plethora of protein aggregates in cerebral amyloidoses. *ACS chemical biology* **4**: 673-684.

Azevedo, E.P., A.B. Guimaraes-Costa, G.S. Torezani, C.A. Braga, F.L. Palhano, J.W. Kelly, E.M. Saraiva & D. Foguel, (2012) Amyloid fibrils trigger the release of neutrophil extracellular traps (NETs), causing fibril fragmentation by NET-associated elastase. *J Biol Chem* **287**: 37206-37218.

Balch, W.E., R.I. Morimoto, A. Dillin & J.W. Kelly, (2008) Adapting proteostasis for disease intervention. *Science* **319**: 916-919.

Bednarska, N.G., J. Schymkowitz, F. Rousseau & J. Van Eldere, (2013) Protein aggregation in Bacteria: the thin boundary betweenfunctionality and toxicity. *Microbiology*.

Benilova, I., E. Karran & B. De Strooper, (2012) The toxic A beta oligomer and Alzheimer's disease: an emperor in need of clothes. *Nature Neuroscience* **15**: 349-357.

Boersma, A.J., I.S. Zuhorn & B. Poolman, (2015) A sensor for quantification of macromolecular crowding in living cells. *Nat Methods* **12**: 227-229, 221 p following 229.

Brogden, K.A., (2005) Antimicrobial peptides: pore formers or metabolic inhibitors in bacteria? *Nat Rev Microbiol* **3**: 238-250.

Campioni, S., B. Mannini, M. Zampagni, A. Pensalfini, C. Parrini, E. Evangelisti, A. Relini, M. Stefani, C.M. Dobson, C. Cecchi & F. Chiti, (2010) A causative link between the structure of aberrant protein oligomers and their toxicity. *Nat Chem Biol* **6**: 140-147.

Chambers, H.F., (2001) Methicillin-resistant Staphylococcus aureus. Mechanisms of resistance and implications for treatment. *Postgraduate medicine* **109**: 43-50.

1 Chaudhuri, R., A. Allen, P. Owen, G. Shalom, K. Stone, M. Harrison, T. Burgis, M.
2 Lockyer, J. Garcia-Lara, S. Foster, S. Pleasance, S. Peters, D. Maskell & I.
3 Charles, (2009) Comprehensive identification of essential Staphylococcus
4 aureus genes using Transposon-Mediated Differential Hybridisation
5 (TMDH). *BMC genomics* **10**: 291.
6 Code, C., Y.A. Domanov, J.A. Killian & P.K. Kinnunen, (2009) Activation of
7 phospholipase A2 by temporin B: formation of antimicrobial peptide-
8 enzyme amyloid-type cofibrils. *Biochim Biophys Acta* **1788**: 1064-1072.
9 De Baets, G., J. Schymkowitz & F. Rousseau, (2014) Predicting aggregation-
10 prone sequences in proteins. *Essays Biochem* **56**: 41-52.
11 Epand, R.M. & R.F. Epand, Bacterial membrane lipids in the action of
12 antimicrobial agents. *Journal of Peptide Science* **17**: 298-305.
13 Esteras-Chopo, A., L. Serrano & M.L. de la Paz, (2005) The amyloid stretch
14 hypothesis: Recruiting proteins toward the dark side. *Proceedings of the*
15 *National Academy of Sciences of the United States of America* **102**: 16672-
16 16677.
17 Evangelisti, E., C. Cecchi, R. Cascella, C. Sgromo, M. Becatti, C.M. Dobson, F. Chiti &
18 M. Stefani, (2012) Membrane lipid composition and its physicochemical
19 properties define cell vulnerability to aberrant protein oligomers. *Journal*
20 *of cell science* **125**: 2416-2427.
21 Fernandez-Escamilla, A.M., F. Rousseau, J. Schymkowitz & L. Serrano, (2004)
22 Prediction of sequence-dependent and mutational effects on the
23 aggregation of peptides and proteins. *Nat Biotechnol* **22**: 1302-1306.
24 Ganesan, A., M. Debulpaep, H. Wilkinson, J. Van Durme, G. De Baets, W.
25 Jonckheere, M. Ramakers, Y. Ivarsson, P. Zimmermann, J. Van Eldere, J.
26 Schymkowitz & F. Rousseau, (2014) Selectivity of aggregation-
27 determining interactions. *Journal of Molecular Biology* **426**.
28 Gravitz, L., (2012) Turning a new phage. *Nat Med* **18**: 1318-1320.
29 Hammarstrom, P., R. Simon, S. Nystrom, P. Konradsson, A. Aslund & K.P. Nilsson,
30 (2010) A fluorescent pentameric thiophene derivative detects in vitro-
31 formed prefibrillar protein aggregates. *Biochemistry* **49**: 6838-6845.
32 Hancock, R.E. & D.S. Chapple, (1999) Peptide antibiotics. *Antimicrobial agents*
33 *and chemotherapy* **43**: 1317-1323.
34 Hartmann, M., M. Berditsch, J. Hawecker, M.F. Ardakani, D. Gerthsen & A.S. Ulrich,
35 (2010) Damage of the bacterial cell envelope by antimicrobial peptides
36 gramicidin S and PGLa as revealed by transmission and scanning electron
37 microscopy. *Antimicrobial agents and chemotherapy* **54**: 3132-3142.
38 Helsens, K., N. Colaert, H. Barsnes, T. Muth, K. Flikka, A. Staes, E. Timmerman, S.
39 Wortelkamp, A. Sickmann, J. Vandekerckhove, K. Gevaert & L. Martens,
40 (2010) ms_lims, a simple yet powerful open source laboratory
41 information management system for MS-driven proteomics. *Proteomics*
42 **10**: 1261-1264.
43 Huang da, W., B.T. Sherman, Q. Tan, J. Kir, D. Liu, D. Bryant, Y. Guo, R. Stephens,
44 M.W. Baseler, H.C. Lane & R.A. Lempicki, (2007) DAVID Bioinformatics
45 Resources: expanded annotation database and novel algorithms to better
46 extract biology from large gene lists. *Nucleic Acids Res* **35**: W169-175.
47 Kall, L., J.D. Storey, M.J. MacCoss & W.S. Noble, (2008) Posterior error
48 probabilities and false discovery rates: two sides of the same coin. *J*
49 *Proteome Res* **7**: 40-44.

Kersey, P.J., D.M. Staines, D. Lawson, E. Kulesha, P. Derwent, J.C. Humphrey, D.S. Hughes, S. Keenan, A. Kerhornou, G. Koscielny, N. Langridge, M.D. McDowall, K. Megy, U. Maheswari, M. Nuhn, M. Paulini, H. Pedro, I. Toneva, D. Wilson, A. Yates & E. Birney, (2012) Ensembl Genomes: an integrative resource for genome-scale data from non-vertebrate species. *Nucleic Acids Res* **40**: D91-97.

Klingstedt, T., A. Aslund, R.A. Simon, L.B. Johansson, J.J. Mason, S. Nystrom, P. Hammarstrom & K.P. Nilsson, (2011) Synthesis of a library of oligothiophenes and their utilization as fluorescent ligands for spectral assignment of protein aggregates. *Organic & biomolecular chemistry* **9**: 8356-8370.

Knappe, D., M. Zahn, U. Sauer, G. Schiffer, N. Strater & R. Hoffmann, (2011) Rational design of oncocin derivatives with superior protease stabilities and antibacterial activities based on the high-resolution structure of the oncocin-DnaK complex. *Chembiochem* **12**: 874-876.

Kristian, S.A., M. Durr, J.A. Van Strijp, B. Neumeister & A. Peschel, (2003) MprF-mediated lysinylation of phospholipids in Staphylococcus aureus leads to protection against oxygen-independent neutrophil killing. *Infect Immun* **71**: 546-549.

Laganowsky, A., C. Liu, M.R. Sawaya, J.P. Whitelegge, J. Park, M. Zhao, A. Pensalfini, A.B. Soriaga, M. Landau, P.K. Teng, D. Cascio, C. Glabe & D. Eisenberg, (2012) Atomic view of a toxic amyloid small oligomer. *Science* **335**: 1228-1231.

Lashuel, H.A. & P.T. Lansbury, Jr., (2006) Are amyloid diseases caused by protein aggregates that mimic bacterial pore-forming toxins? *Q Rev Biophys* **39**: 167-201.

Last, N.B. & A.D. Miranker, (2013) Common mechanism unites membrane poration by amyloid and antimicrobial peptides. *Proc Natl Acad Sci U S A* **110**: 6382-6387.

Lee, J. & D.G. Lee, (2014) Antimicrobial Peptides (AMPs) with Dual Mechanisms: Membrane Disruption and Apoptosis. *J Microbiol Biotechnol*.

Lesne, S., M.T. Koh, L. Kotilinek, R. Kayed, C.G. Glabe, A. Yang, M. Gallagher & K.H. Ashe, (2006) A specific amyloid-beta protein assembly in the brain impairs memory. *Nature* **440**: 352-357.

Li, Z., X. Xu, L. Meng, Q. Zhang, L. Cao, W. Li, Y. Wu & Z. Cao, (2014) Hp1404, a new antimicrobial peptide from the scorpion Heterometrus petersii. *PLoS One* **9**: e97539.

Lindner, A.B., R. Madden, A. Demarez, E.J. Stewart & F.o. Taddei, (2008) Asymmetric segregation of protein aggregates is associated with cellular aging and rejuvenation. *Proceedings of the National Academy of Sciences* **105**: 3076-3081.

Livermore, D.M., (2011) Discovery research: the scientific challenge of finding new antibiotics. *The Journal of antimicrobial chemotherapy* **66**: 1941-1944.

Mahalka, A.K. & P.K. Kinnunen, (2009) Binding of amphipathic alpha-helical antimicrobial peptides to lipid membranes: lessons from temporins B and L. *Biochim Biophys Acta* **1788**: 1600-1609.

Matsuzaki, K., (1998) Magainins as paradigm for the mode of action of pore forming polypeptides. *Biochimica et Biophysica Acta (BBA) - Reviews on Biomembranes* **1376**: 391-400.

Mitulovic, G., C. Stingl, I. Steinmacher, O. Hudecz, J.R. Hutchins, J.M. Peters & K. Mechtler, (2009) Preventing carryover of peptides and proteins in nano LC-MS separations. *Analytical chemistry* **81**: 5955-5960.

Morales, R., I. Moreno-Gonzalez & C. Soto, (2013) Cross-seeding of misfolded proteins: implications for etiology and pathogenesis of protein misfolding diseases. *PLoS pathogens* **9**: e1003537.

Munch, C., J. O'Brien & A. Bertolotti, (2011) Prion-like propagation of mutant superoxide dismutase-1 misfolding in neuronal cells. *Proc Natl Acad Sci U S A* **108**: 3548-3553.

Nakatsuji, T. & R.L. Gallo, (2012) Antimicrobial peptides: old molecules with new ideas. *The Journal of investigative dermatology* **132**: 887-895.

Narayanan, S., B. Bosl, S. Walter & B. Reif, (2003) Importance of low-oligomeric-weight species for prion propagation in the yeast prion system Sup35/Hsp104. *Proc Natl Acad Sci U S A* **100**: 9286-9291.

Nguyen, L.T., E.F. Haney & H.J. Vogel, The expanding scope of antimicrobial peptide structures and their modes of action. *Trends in Biotechnology* **29**: 464-472.

Nizet, V., A.L. Smith, P.M. Sullam & C.E. Rubens, (1998) A simple microtiter plate screening assay for bacterial invasion or adherence. In: Methods for studying the genetics, molecular biology, physiology, and pathogenesis of the streptococci. Springer, pp. 107-111.

Olzscha, H., S.M. Schermann, A.C. Woerner, S. Pinkert, M.H. Hecht, G.G. Tartaglia, M. Vendruscolo, M. Hayer-Hartl, F.U. Hartl & R.M. Vabulas, (2011) Amyloid-like aggregates sequester numerous metastable proteins with essential cellular functions. *Cell* **144**: 67-78.

Ono, K., R. Takahashi, T. Ikeda & M. Yamada, (2012) Cross-seeding effects of amyloid beta-protein and alpha-synuclein. *J Neurochem* **122**: 883-890.

Peschel, A., R.W. Jack, M. Otto, L.V. Collins, P. Staubitz, G. Nicholson, H. Kalbacher, W.F. Nieuwenhuizen, G. Jung, A. Tarkowski, K.P. van Kessel & J.A. van Strijp, (2001) Staphylococcus aureus resistance to human defensins and evasion of neutrophil killing via the novel virulence factor MprF is based on modification of membrane lipids with l-lysine. *The Journal of experimental medicine* **193**: 1067-1076.

Pootoolal, J., J. Neu & G.D. Wright, (2002) Glycopeptide antibiotic resistance. *Annu Rev Pharmacol Toxicol* **42**: 381-408.

Powers, J.-P.S. & R.E.W. Hancock, (2003) The relationship between peptide structure and antibacterial activity. *Peptides* **24**: 1681-1691.

Ren, P.H., J.E. Lauckner, I. Kachirskaia, J.E. Heuser, R. Melki & R.R. Kopito, (2009) Cytoplasmic penetration and persistent infection of mammalian cells by polyglutamine aggregates. *Nat Cell Biol* **11**: 219-225.

Rokney, A., M. Shagan, M. Kessel, Y. Smith, I. Rosenshine & A.B. Oppenheim, (2009) E. coli Transports Aggregated Proteins to the Poles by a Specific and Energy-Dependent Process. *Journal of Molecular Biology* **392**: 589-601.

Rousseau, F., J. Schymkowitz & L. Serrano, (2006a) Protein aggregation and amyloidosis: confusion of the kinds? *Current Opinion in Structural Biology* **16**: 118-126.

Rousseau, F., L. Serrano & J.W.H. Schymkowitz, (2006b) How evolutionary pressure against protein aggregation shaped chaperone specificity. *Journal of Molecular Biology* **355**: 1037-1047.

Roy, R.N., I.B. Lomakin, M.G. Gagnon & T.A. Steitz, (2015) The mechanism of inhibition of protein synthesis by the proline-rich peptide oncocin. *Nat Struct Mol Biol* **22**: 466-469.

Sabate, R. & S.J. Saupe, (2007) Thioflavin T fluorescence anisotropy: An alternative technique for the study of amyloid aggregation. *Biochem Biophys Res Commun* **360**: 135-138.

Schuller, F., R. Benz & H.G. Sahl, (1989) The peptide antibiotic subtilin acts by formation of voltage-dependent multi-state pores in bacterial and artificial membranes. *European journal of biochemistry / FEBS* **182**: 181-186.

Seefeldt, A.C., F. Nguyen, S. Antunes, N. Perebaskine, M. Graf, S. Arenz, K.K. Inampudi, C. Douat, G. Guichard, D.N. Wilson & C.A. Innis, (2015) The proline-rich antimicrobial peptide Onc112 inhibits translation by blocking and destabilizing the initiation complex. *Nat Struct Mol Biol* **22**: 470-475.

Shai, Y., (2002) Mode of action of membrane active antimicrobial peptides. *Biopolymers* **66**: 236-248.

Shankar, G.M., S. Li, T.H. Mehta, A. Garcia-Munoz, N.E. Shepardson, I. Smith, F.M. Brett, M.A. Farrell, M.J. Rowan, C.A. Lemere, C.M. Regan, D.M. Walsh, B.L. Sabatini & D.J. Selkoe, (2008) Amyloid-beta protein dimers isolated directly from Alzheimer's brains impair synaptic plasticity and memory. *Nat Med* **14**: 837-842.

Soscia, S.J., J.E. Kirby, K.J. Washicosky, S.M. Tucker, M. Ingelsson, B. Hyman, M.A. Burton, L.E. Goldstein, S. Duong, R.E. Tanzi & R.D. Moir, (2010) The Alzheimer's disease-associated amyloid beta-protein is an antimicrobial peptide. *PLoS One* **5**: e9505.

Spitzer, J. & B. Poolman, (2013) How crowded is the prokaryotic cytoplasm? *FEBS Lett* **587**: 2094-2098.

Torrent, M., J. Valle, M.V. Nogués, E. Boix & D. Andreu, (2011) The Generation of Antimicrobial Peptide Activity: A Trade-off between Charge and Aggregation? *Angewandte Chemie* **123**: 10874-10877.

Venyaminov, S. & N.N. Kalnin, (1990) Quantitative IR spectrophotometry of peptide compounds in water (H2O) solutions. II. Amide absorption bands of polypeptides and fibrous proteins in alpha-, beta-, and random coil conformations. *Biopolymers* **30**: 1259-1271.

Waghu, F.H., L. Gopi, R.S. Barai, P. Ramteke, B. Nizami & S. Idicula-Thomas, (2014) CAMP: Collection of sequences and structures of antimicrobial peptides. *Nucleic Acids Res* **42**: D1154-1158.

Wang, G., X. Li & Z. Wang, (2009) APD2: the updated antimicrobial peptide database and its application in peptide design. *Nucleic Acids Res* **37**: D933-937.

Wu, M., E. Maier, R. Benz & R.E. Hancock, (1999) Mechanism of interaction of different classes of cationic antimicrobial peptides with planar bilayers

and with the cytoplasmic membrane of Escherichia coli. *Biochemistry* **38**: 7235-7242.

Xu, J., J. Reumers, J.R. Couceiro, F. De Smet, R. Gallardo, S. Rudyak, A. Cornelis, J. Rozenski, A. Zwolinska, J.-C. Marine, D. Lambrechts, Y.-A. Suh, F. Rousseau & J. Schymkowitz, (2011) Gain of function of mutant p53 by coaggregation with multiple tumor suppressors. *Nature chemical biology* **7**: 285-295.

Yeaman, M.R. & N.Y. Yount, (2003) Mechanisms of antimicrobial peptide action and resistance. *Pharmacol Rev* **55**: 27-55.

Zhao, H., R. Sood, A. Jutila, S. Bose, G. Fimland, J. Nissen-Meyer & P.K. Kinnunen, (2006) Interaction of the antimicrobial peptide pheromone Plantaricin A with model membranes: implications for a novel mechanism of action. *Biochim Biophys Acta* **1758**: 1461-1474.

Figure Legends

Figure 1. Aggregating bactericidal peptides

(1A) MIC (minimal inhibitory concentration) and MBC (minimal bactericidal concentration) of aggregating peptides and their scrambled versions compared to that of reference antibiotics. **(1B)** Resistance development curve for *S. aureus* ATCC type strain nr 29213 evaluated by repeated passaging over a period of 15 days and MIC determination. Data points represent the median of 3 replicates with error bars showing the range. **(1C)** Resistance development curve for Methicillin resistant *S. aureus* strain 326 sub-cultured in a medium supplemented with sub-inhibitory concentrations of peptides over a period of 32 days assessed by daily monitoring of the MIC level. Data points represent median of 3 replicates with error bars showing the range. **(1D)** Receiver-Operator Curve of the predictive power of individual proteome sequence-derived parameters on the species specificity of the peptides. **(1E)** The killing kinetics of Methicillin resistant *S. aureus* strain 326 treated with 2 x MIC concentrations of peptides. Viable cells were quantified at different time points of treatment and expressed as the Log of Colony Forming Units.mL^{-1}.

Figure 2. Bactericidal peptides form peptide aggregates.

(2A) TEM micrograph of aggregating peptides after incubation for 1 month at 37ºC at stock concentrations (1.0, 0.5, 0.08 and 0.8 mM for C29, C30, Hit1 and Hit50). **(2B)** Aggregation kinetic of aggregating peptides as monitored by DLS. All peptides were at 50 μM. **(2C)** CD spectroscopy and **(2D)** FT-IR spectroscopy analysis of aggregated peptides after 1 week incubation at 37ºC. All peptides were at 50 μM.

Figure 3. Aggregating bactericidal peptides are internalized and induce intracbacterial protein aggregation.

(3A) Flow cytometry analysis of LCP (FITC channel 458/480nm, x axis) versus PI (PE-A channel 535/617nm, y axis) stained Methicillin resistant S. aureus strain 326 treated with C30, Hit50 and vancomycin. Treatment with peptides shows strong increase in both PI and LCP signal, while vancomycin treatment leads to

increase of PI signal only. **(3B)** Overlaid spectra of peptide and scrambled peptide treated *S. aureus* show that scrambled peptide treatment also leads to increase in LCP signal. **(3C)** LCP-positive cells were sorted out and plated for viability assay. For each treatment 100.000 events were collected. P values were calculated via student t-test with Bonferonni's multiple comparison post testing (* $p < 0.05$, ** $p < 0.01$). **(3D)** Summary of bacterial proteins found to change in solubility after peptide treatment.

Figure 4. Aggregating peptides are toxic to bacteria but not to mammalian cells and cure bacterial sepsis in mice

(4A and 4B) Invasion of Methicillin resistant *S. aureus* 326 in a monolayer of human HCT116 cells. Images show four different channels and their overlay: propidium iodide stains dead cells (red channel), CellMask stains the plasma membrane (blue channel), peptide C30 is labelled with DyLight (green channel). **(4A)** Monolayer of infected, untreated HCT116 cell line. Propidium iodide stains of dead cells (upper left quadrant), CellMask stain of the plasma membrane (upper right quadrant), the merged image (lower left quadrant) shows apoptotic cells, the bright-field image (lower right quadrant) shows a heavy load of proliferating bacteria and disturbed morphology of the HCT116 mammalian cells. **(4B)** Monolayer of infected HCT116 cells treated with peptide C30. Upper left quadrant: DyLight-conjugated (green channel) peptide C30 (at a final concentration of 12.5 $\mu g.mL^{-1}$). Upper right quadrant: propidium iodide stains nuclei of dead bacterial cells. Lower right quadrant: merged channels show co-localization of peptides with dead bacterial cells (Pearson's correlation of 0.41 and an overlap score of 0.94); Cell mask stains membrane of healthy, intact cells. Bright-field channel (lower left quadrant) shows decreased amount of bacteria upon treatment. **(4C)** The healthy, intact HCT116 cell monolayer sub-cultured with DyeLight-labelled peptide C30 (2x MIC) for 72 hours shows full recovery (upper half). The Z stack (lower half) shows the intracellular localization of peptide. **(4D)** Number of intracellular bacteria residing in the infected HCT116 cell line after treatment with different concentrations of peptide C30 or vancomycin as a control. Viable intracellular bacteria were enumerated via agar plating method and expressed as Log Colony Forming Units per mL. Error bars

represent the standard error of the mean of triplicates. **(4E)** Hemolytic activities of peptides assessed by monitoring the release of hemoglobin by measuring absorbance at 414 nm. Hemolysis was calculated as the percentage of the hemolysis achieved by 0.1% Tween X-100. Active peptides at their MIC levels exhibit minor hemolysis. The error bars represents standard error of the mean of 4 independent replicates. **(4F)** The effect of peptides on viability of the human colon carcinoma HCT116 cell line monitored by the colorimetric AlamarBlue assay. The error bars represent standard error of the mean of 4 independent samples. **(4G)** Survival curves of *S. aureus* (MRSA326) infected mice treated with a single intravenous dose of peptide C29 (10 $mg.kg^{-1}$), C30 (15 $mg.kg^{-1}$) and Hit50 (5 $mg.kg^{-1}$). A single intravenous vancomycin injection at a concentration of 15 $mg.kg^{-1}$ was given as a control. Data represents 20 animals per group and was analyzed using the log-rank test (by means of Prism 4 software) with P values of <0.0001 for each peptide treatment.

Bednarska et al, Figure 1

A Minimum inhibitory and bactericidal concentrations for *S. epidermidis* ATCC12228

Peptide name	MIC [µg/mL]	MBC[µg/mL]	MIC scrambled [µg/mL]
C30	1.5	1.5	25
C29	0.75	1.5	>200
Hit1	3	3	50
Hit50	6	12.5	>200
Vancomycin	1	1	
Gentamycin	1.5	1.5	
Spectinomycin	25	25	

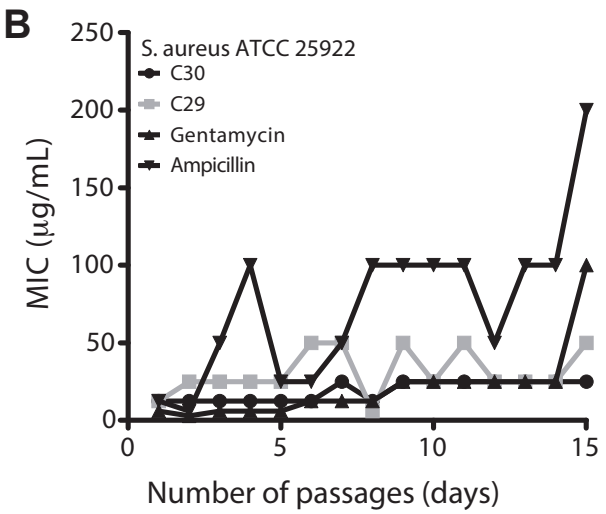

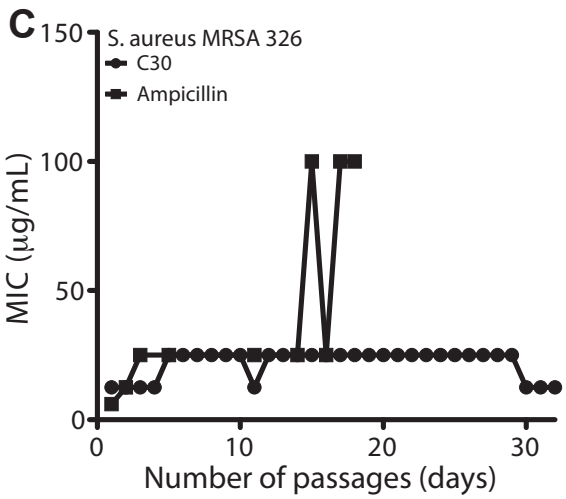

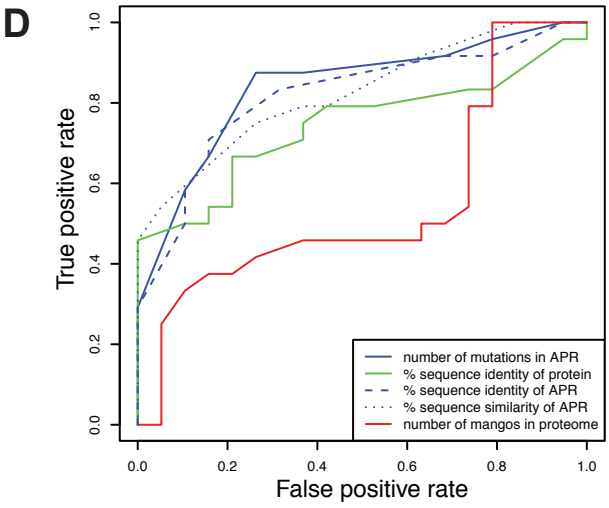

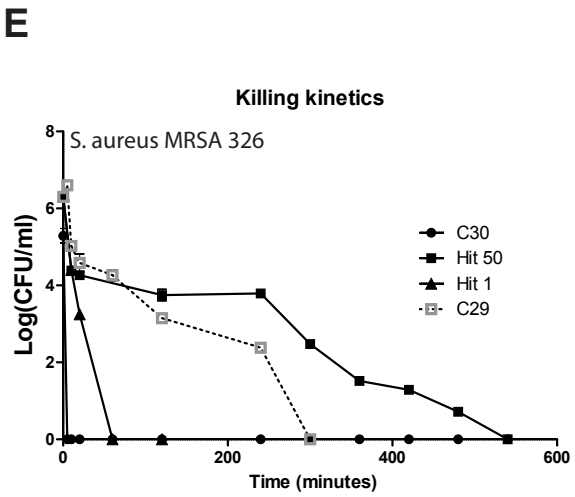

Bednarska et al, Figure 2

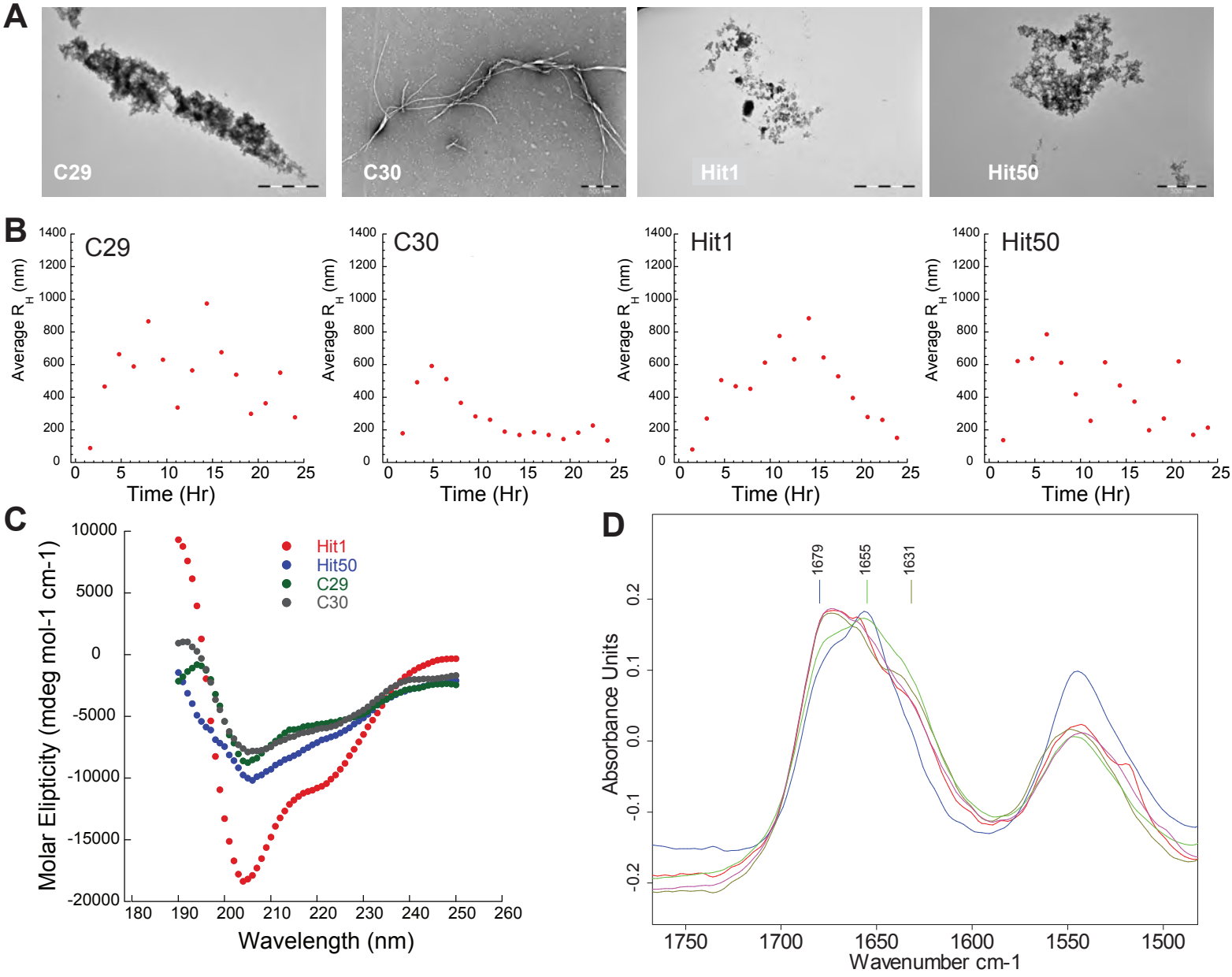

Bednarska et al, Figure 3

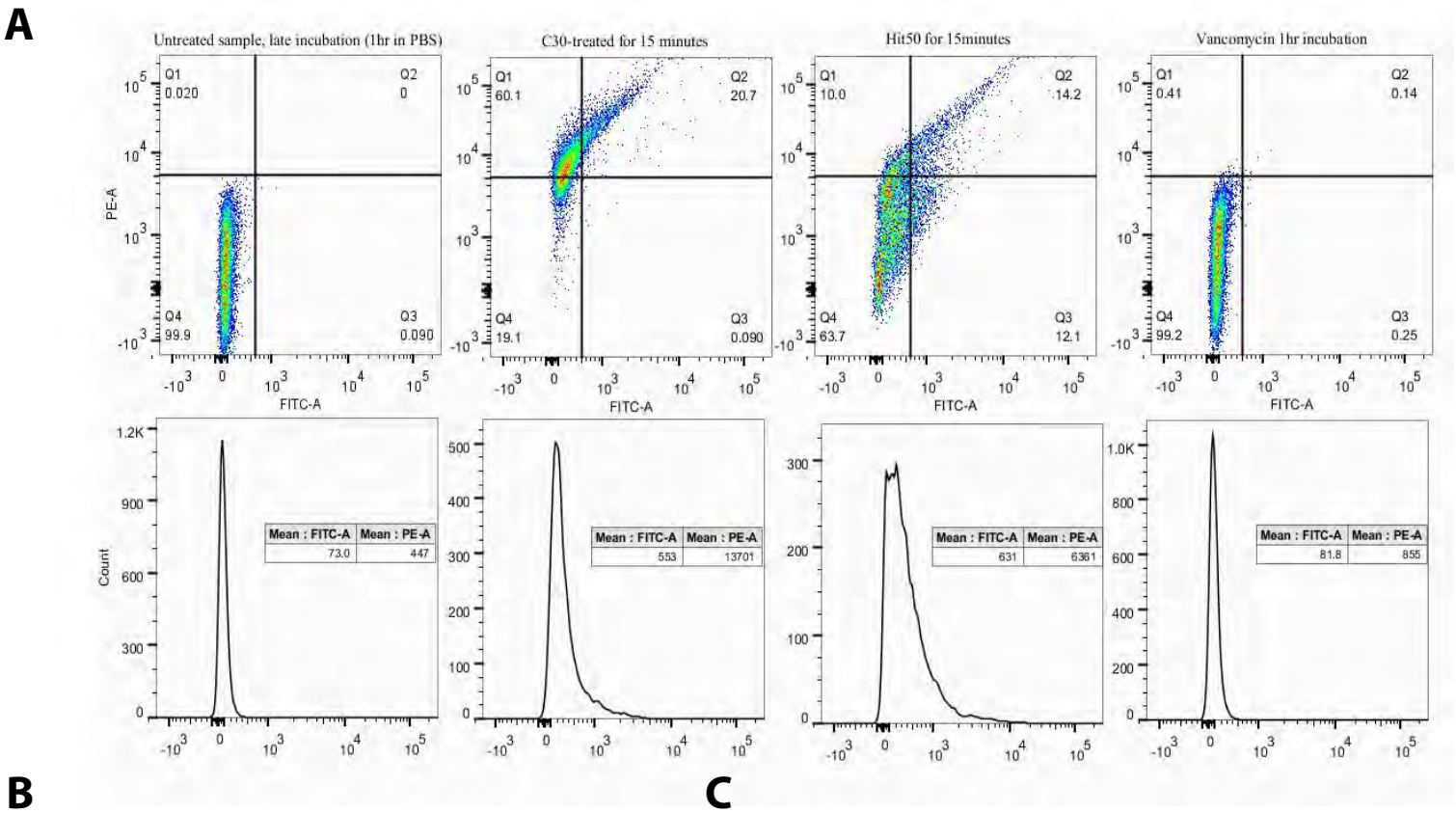

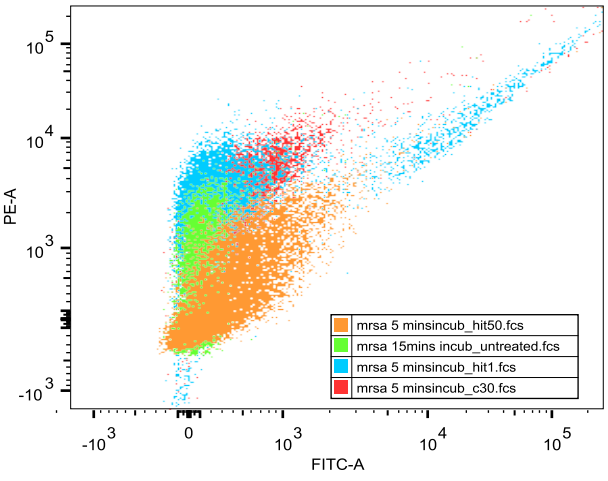

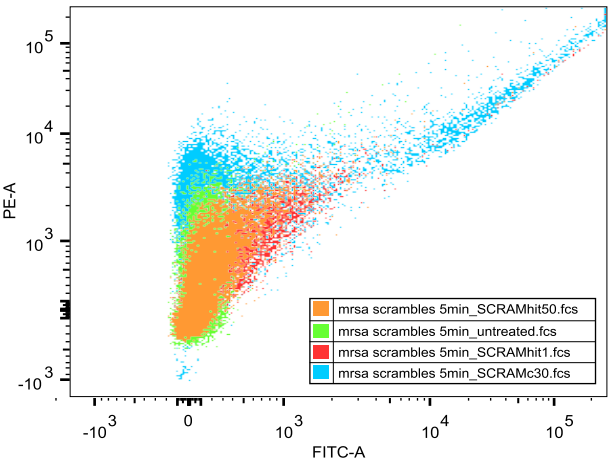

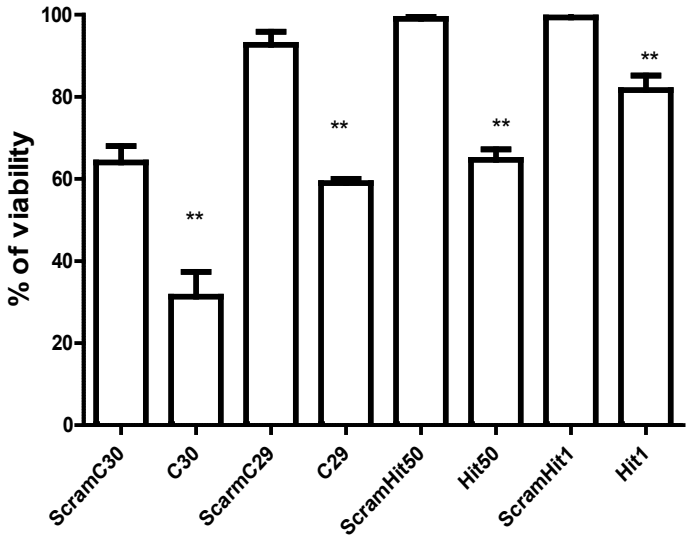

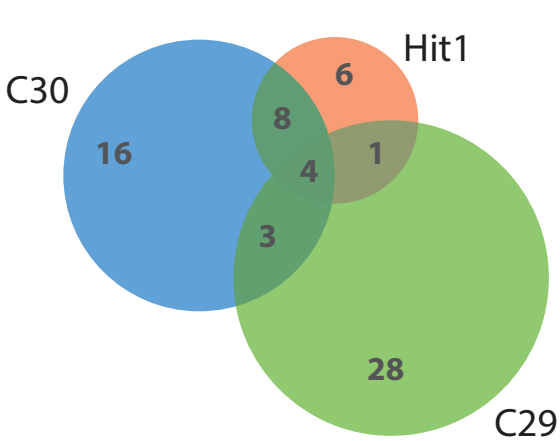

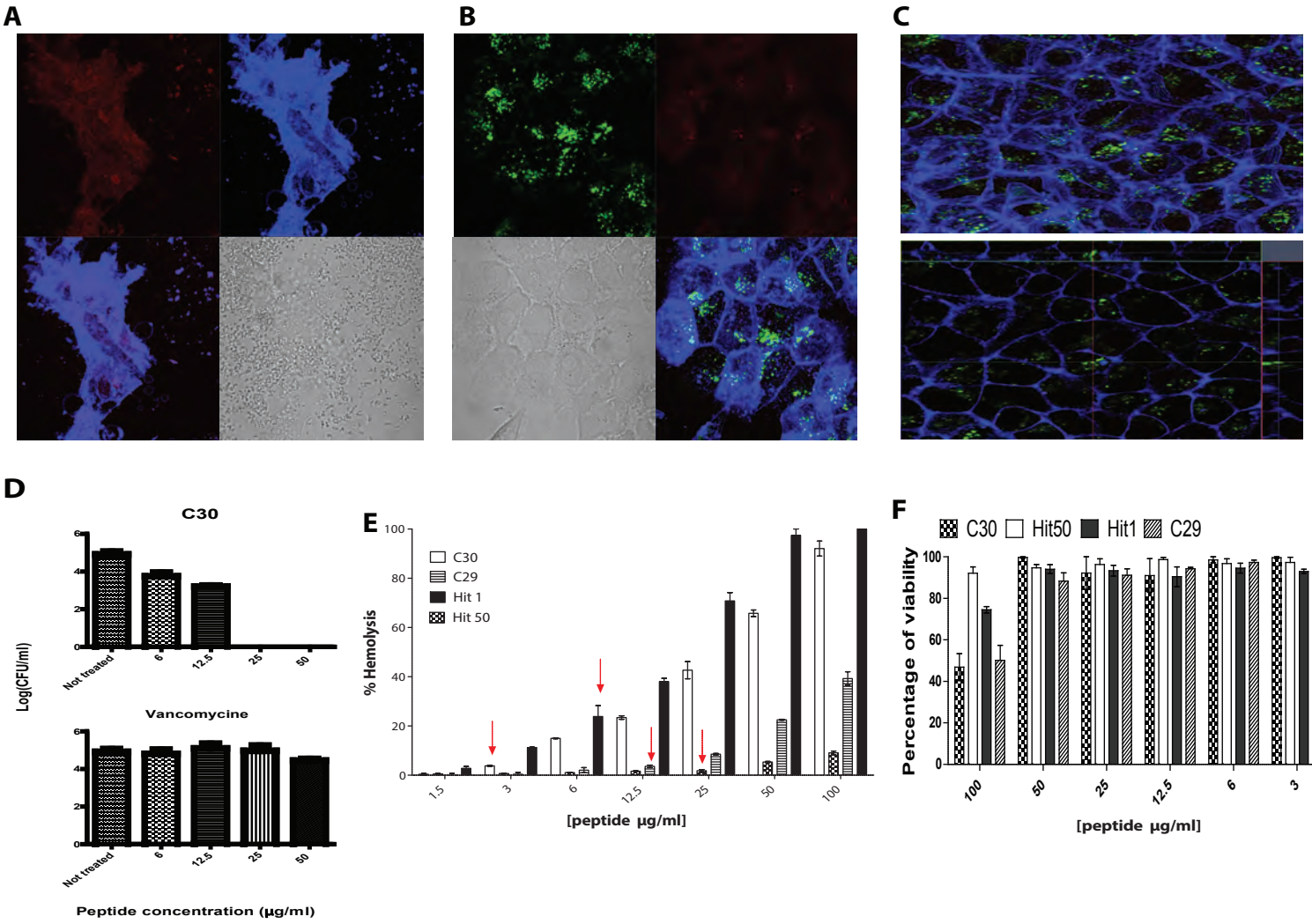

Bednarska et al -Figure 4

Bednarska et al, Supplementary Figure 1

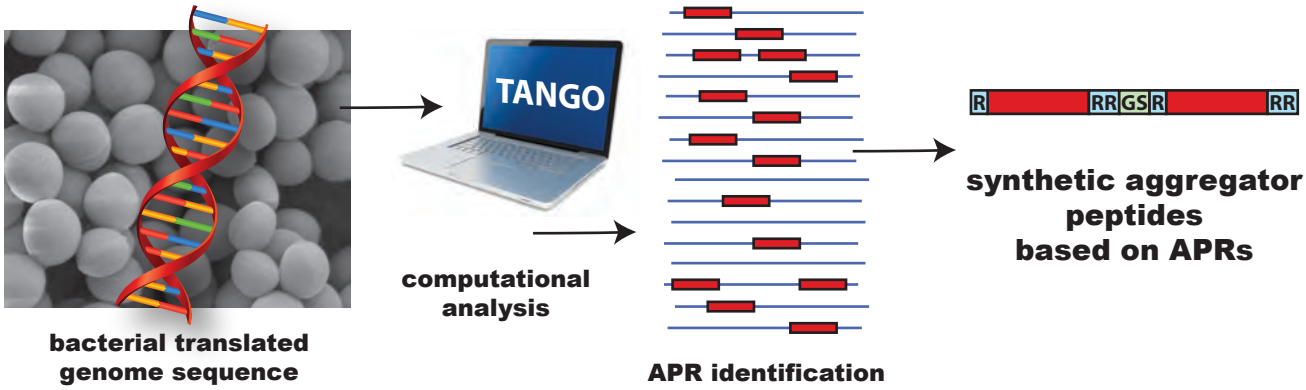

Bednarska et al, Supplementary Figure 4

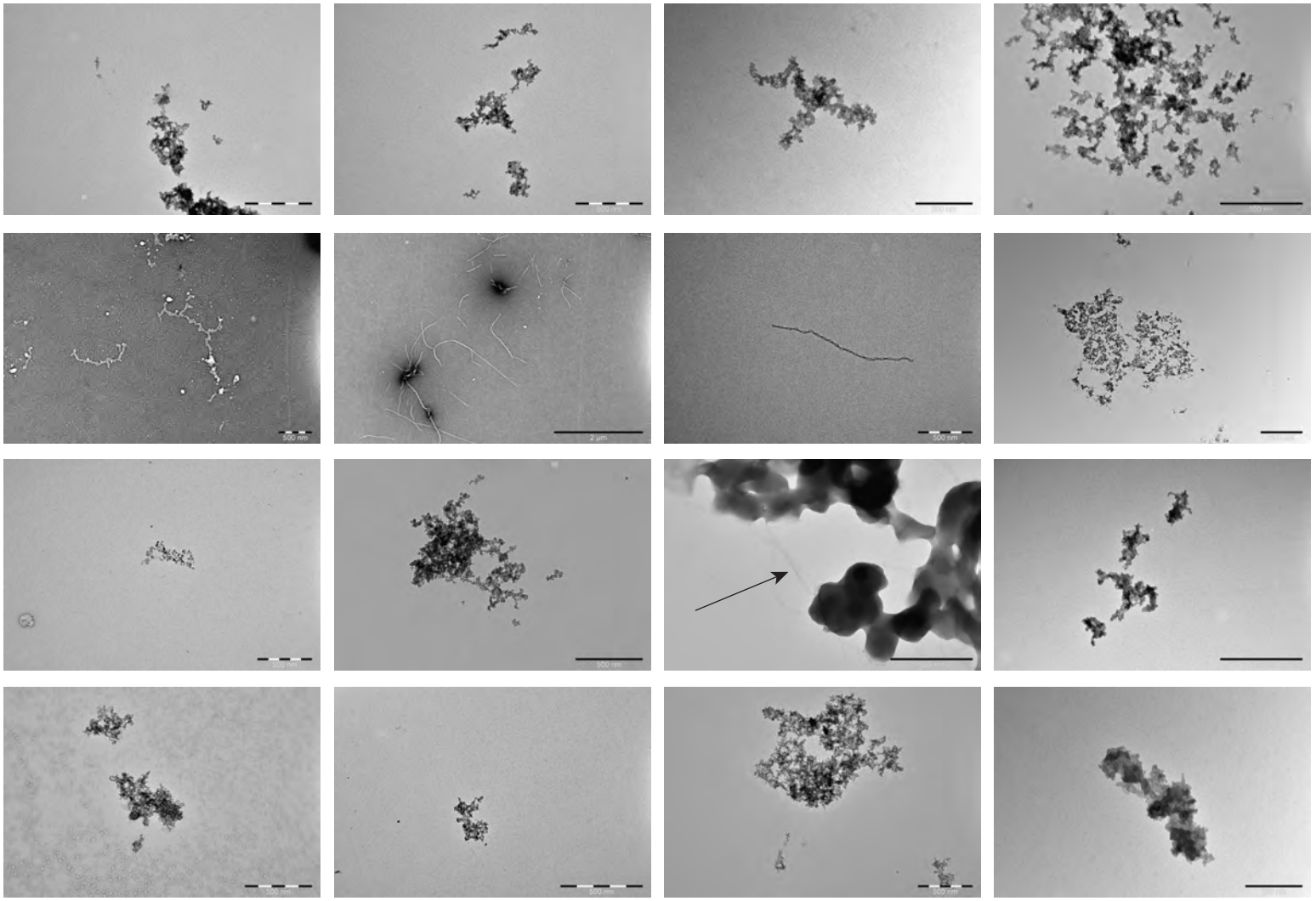

Bednarska et al, Supplementary Figure 3

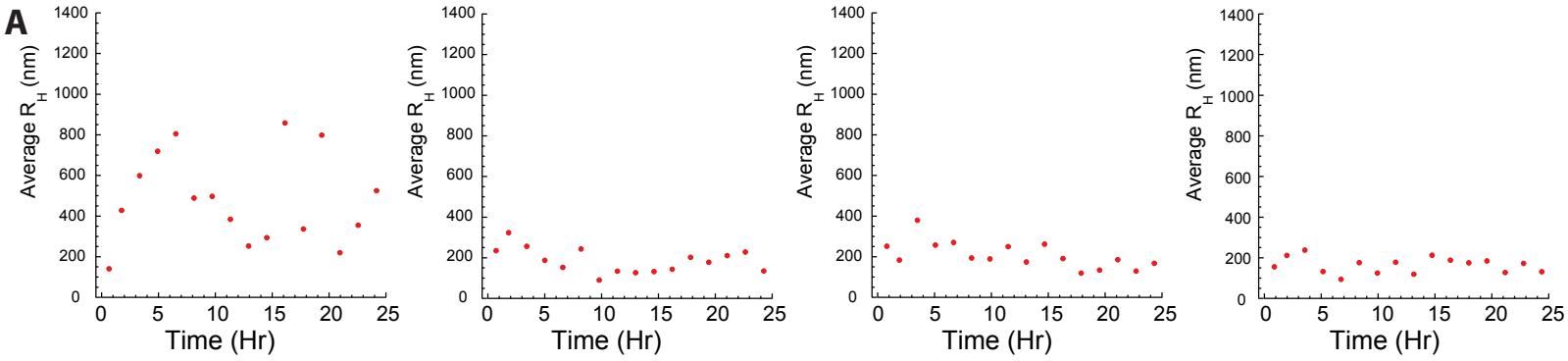

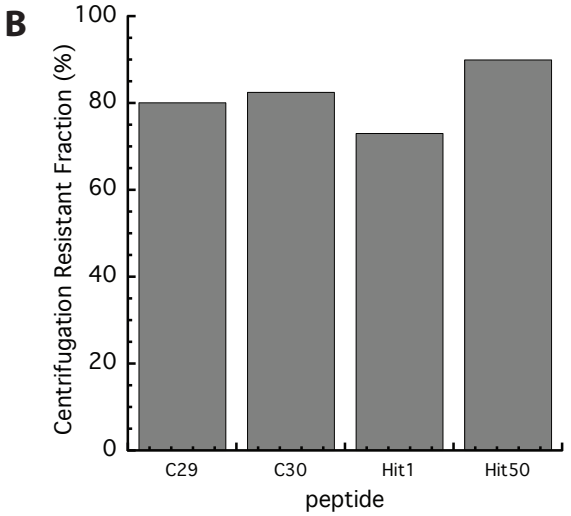

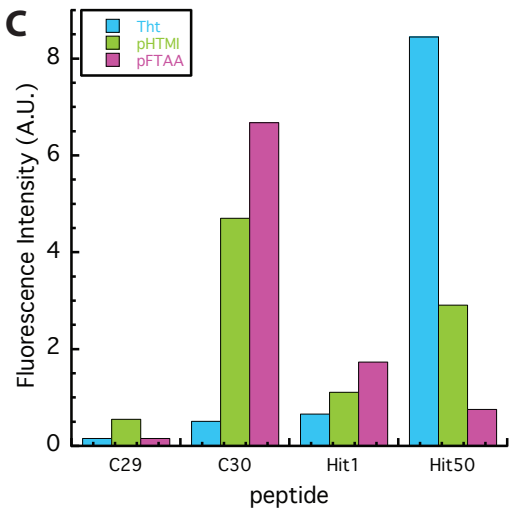

D

Bednarska et al, Supplementary Figure 4

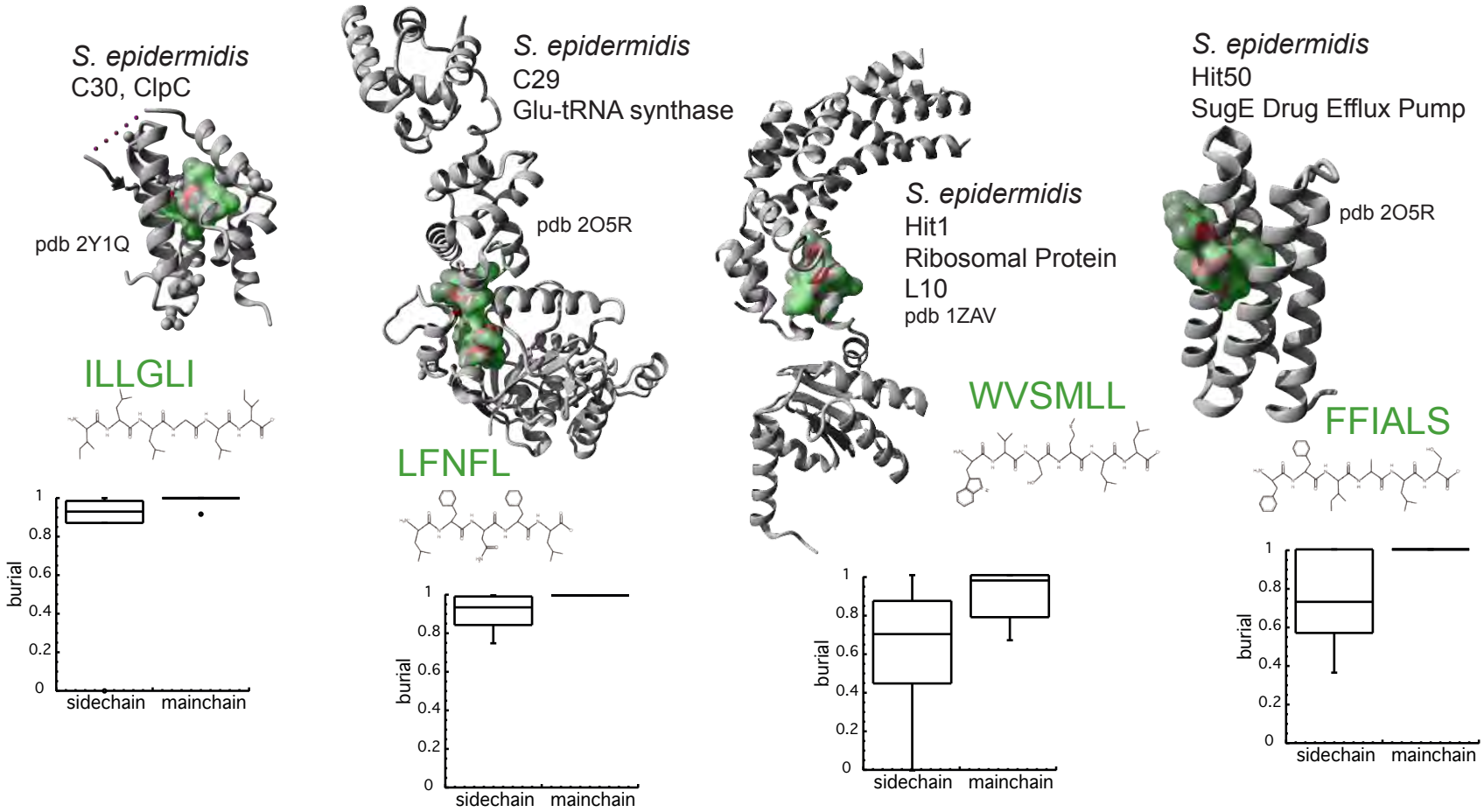

A

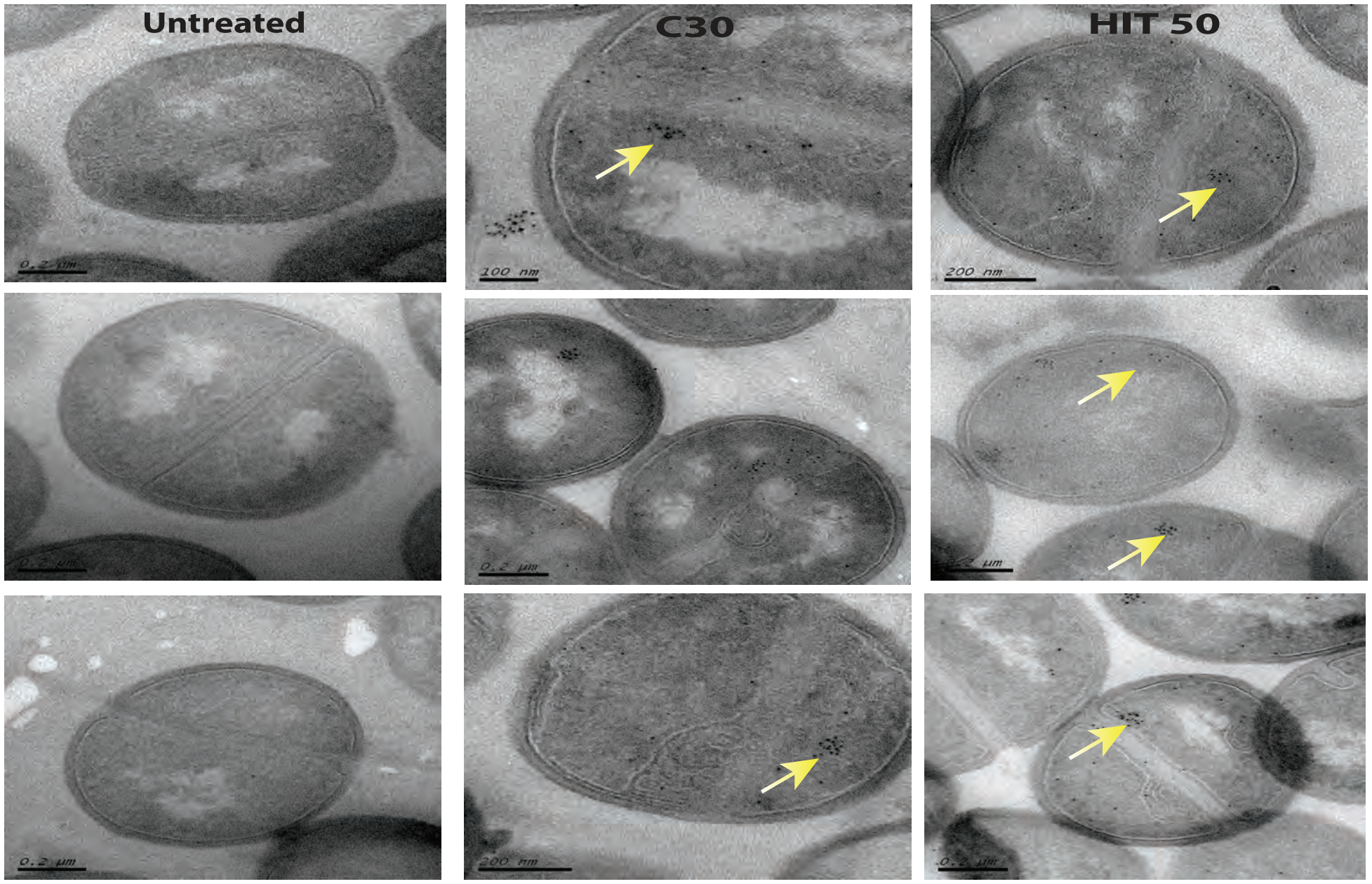

B

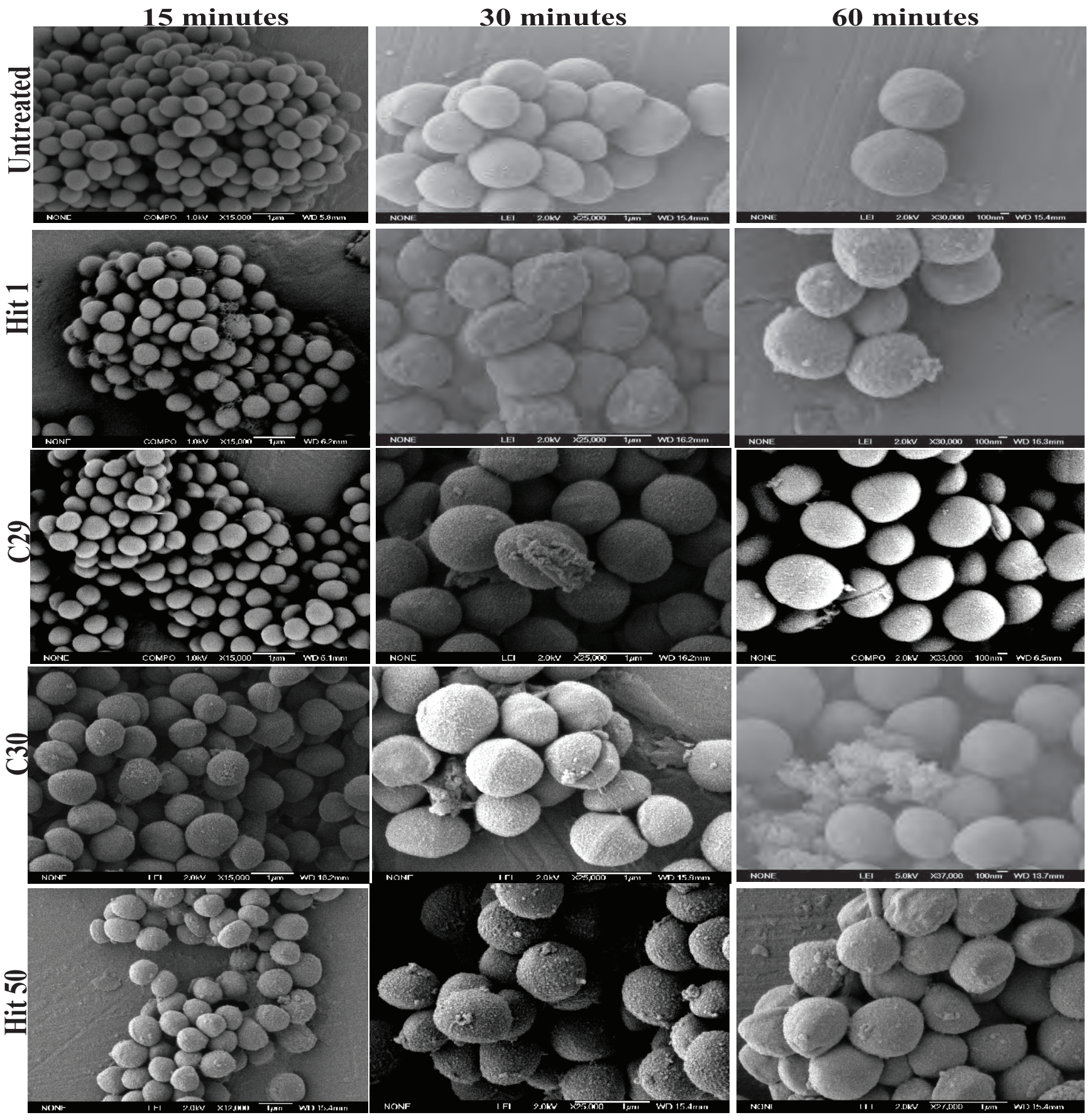

Bednarska et at- Supplementary Figure 5

Bednarska et al, Supplementary Figure 6

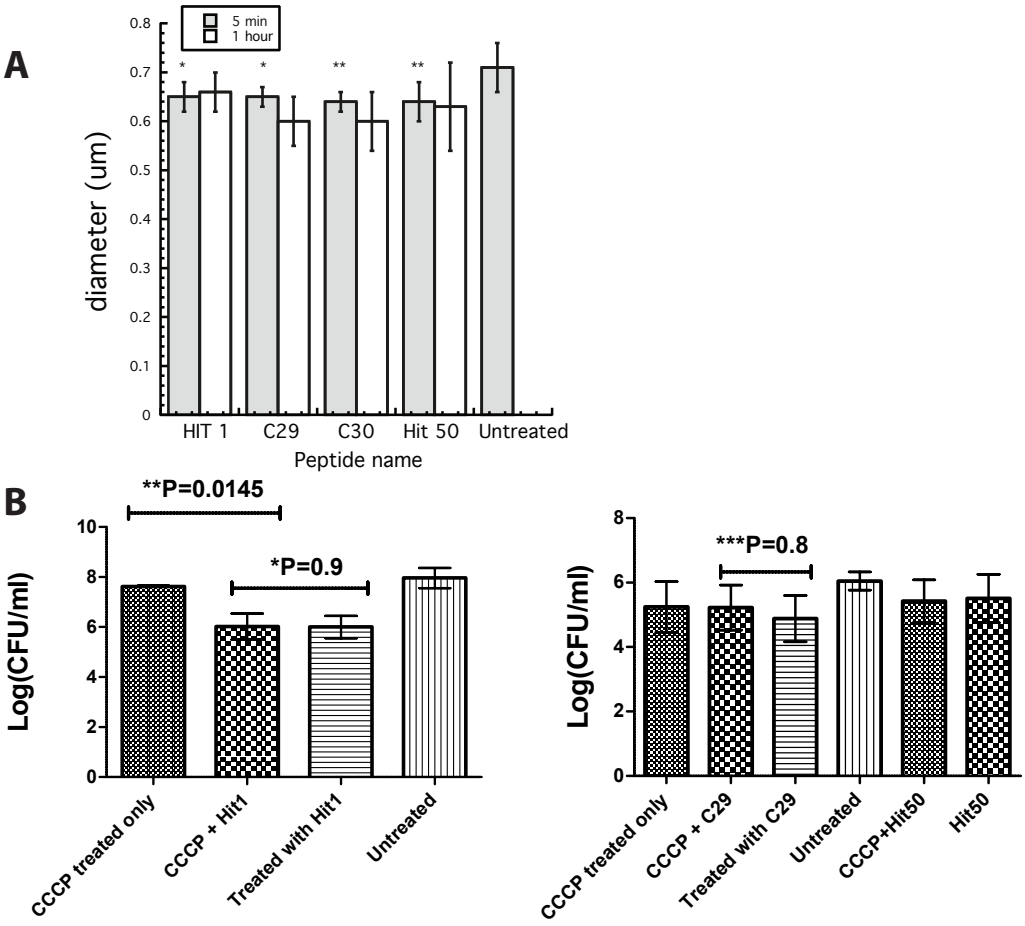

Bednarska et al, Supplementary Figure 7

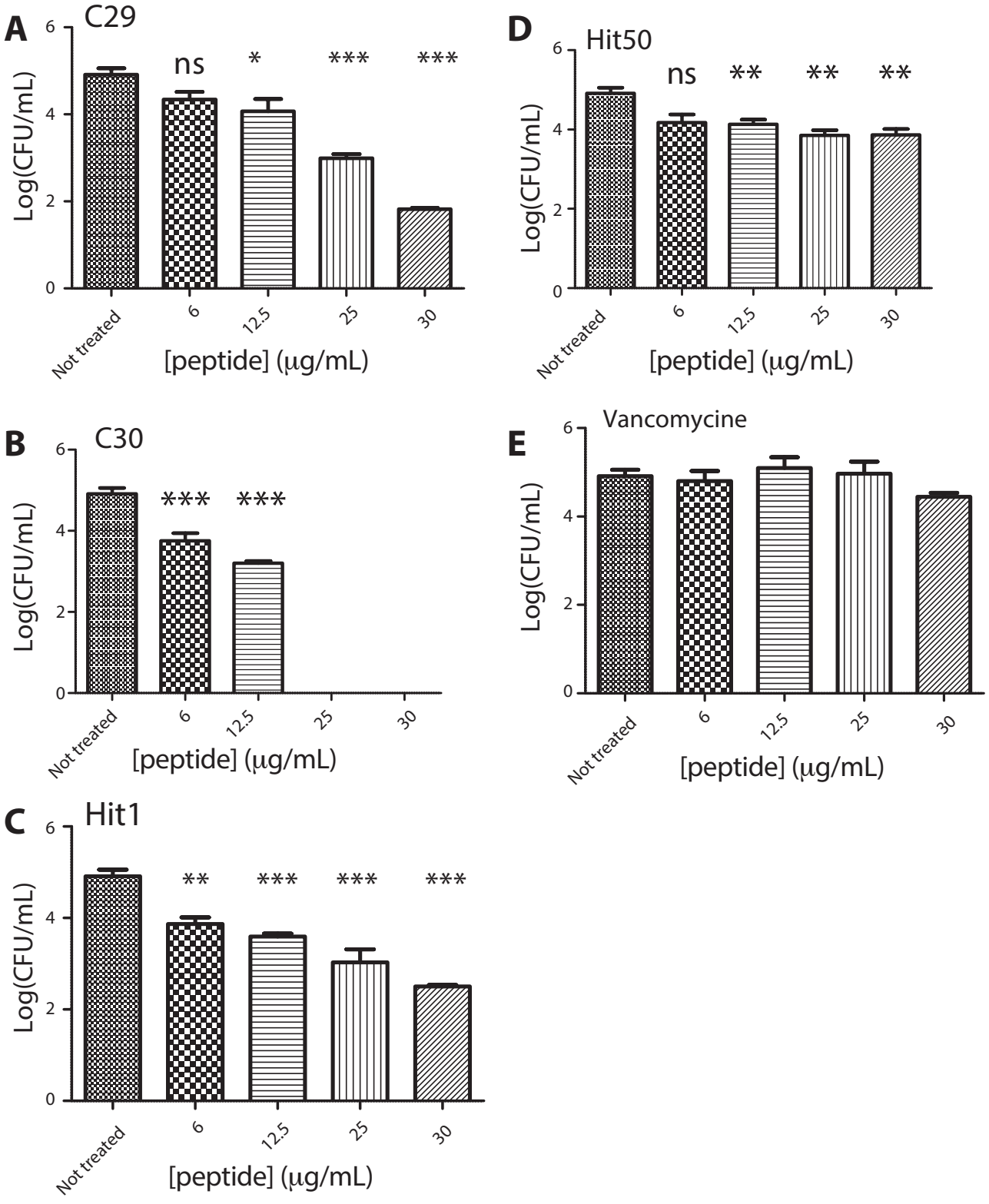

Bednarska et al, Supplementary Figure 8

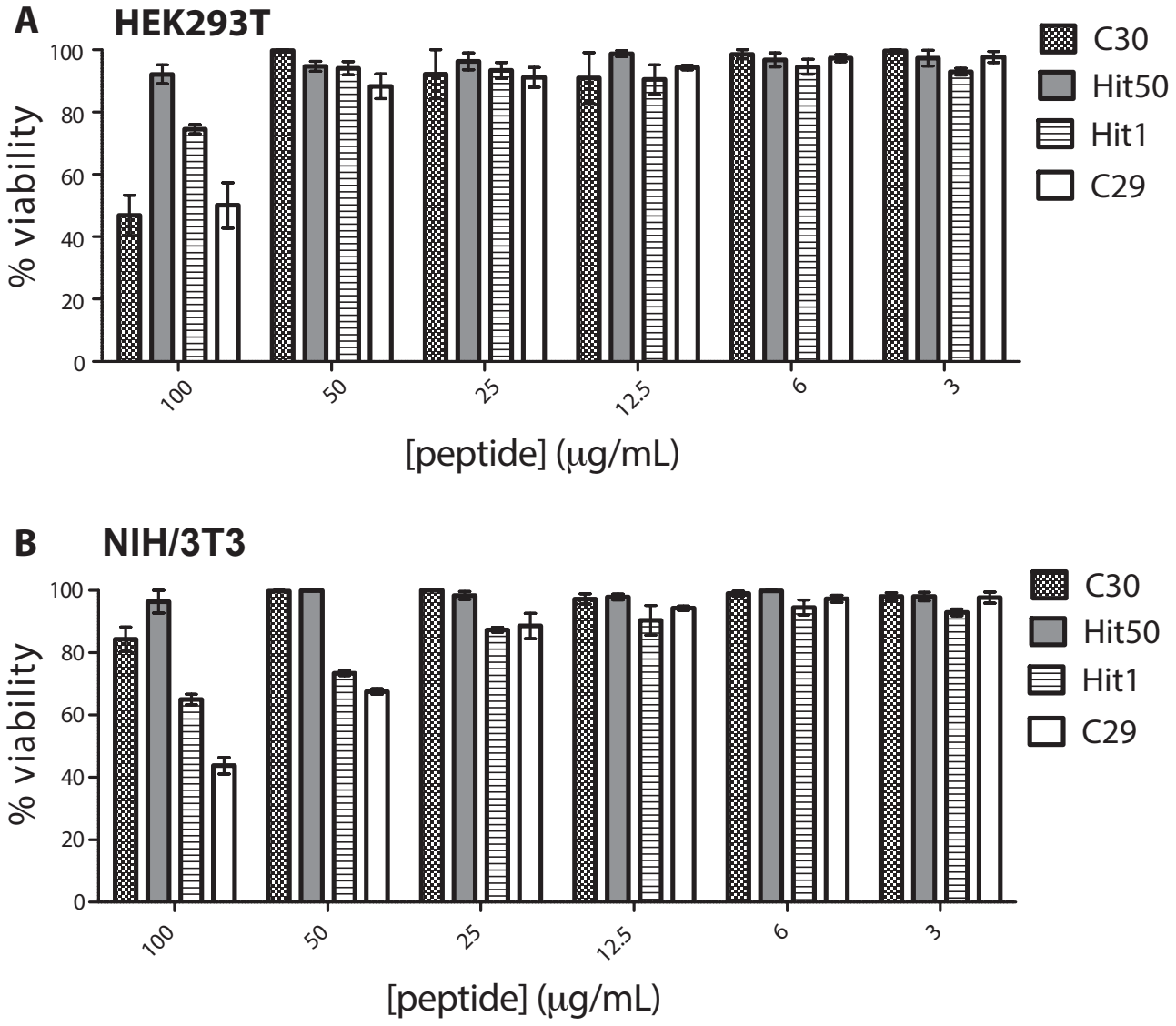

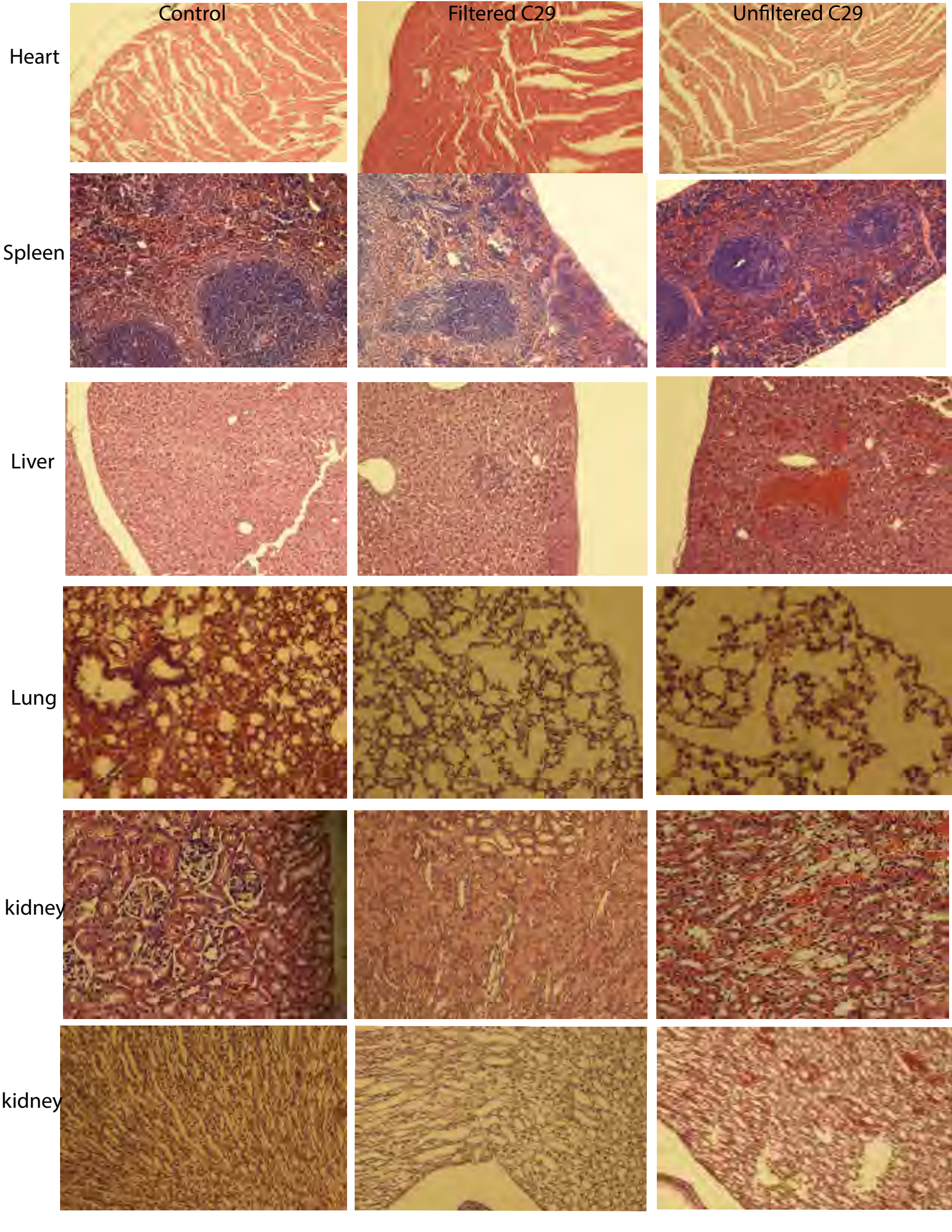
Control
Filtered C29
Unfiltered C29
Heart
Spleen
Liver
Lung
kidney
kidney